



HAL
open science

Environmental and climatic controls of the clay mineralogy of Albian deposits in the Paris and Vocontian basins (France).

Pauline Corentin, Jean-François Deconinck, Pierre Pellenard, Francis Amédro, Ludovic Bruneau, Elise Chenot, Bertrand Matrion, Emilia Huret, Philippe Landrein

► To cite this version:

Pauline Corentin, Jean-François Deconinck, Pierre Pellenard, Francis Amédro, Ludovic Bruneau, et al.. Environmental and climatic controls of the clay mineralogy of Albian deposits in the Paris and Vocontian basins (France).. *Cretaceous Research*, 2020, 108, pp.104342. 10.1016/j.cretres.2019.104342 . hal-02436436

HAL Id: hal-02436436

<https://hal.science/hal-02436436v1>

Submitted on 21 Jul 2022

HAL is a multi-disciplinary open access archive for the deposit and dissemination of scientific research documents, whether they are published or not. The documents may come from teaching and research institutions in France or abroad, or from public or private research centers.

L'archive ouverte pluridisciplinaire **HAL**, est destinée au dépôt et à la diffusion de documents scientifiques de niveau recherche, publiés ou non, émanant des établissements d'enseignement et de recherche français ou étrangers, des laboratoires publics ou privés.



Distributed under a Creative Commons Attribution - NonCommercial 4.0 International License

1 **Environmental and climatic controls of the clay mineralogy of Albian deposits in**
2 **the Paris and Vocontian basins (France)**

3 Pauline CORENTIN ¹, Jean-François DECONINCK ¹ Pierre PELLENARD ¹,
4 Francis AMÉDRO (^{1,2}), Ludovic BRUNEAU ¹, Elise CHENOT (^{1,3}), Bertrand
5 MATRION (^{1,4}), Emilia HURET ⁵ and Philippe LANDREIN ⁵

6 (1) Université de Bourgogne-Franche-Comté, UMR 6282, CNRS, Biogéosciences, 6
7 boulevard Gabriel, 21000 Dijon, France. E-mail: pauline.corentin@u-bourgogne.fr

8 (2) 26 rue de Nottingham, 62100 Calais, France.

9 (3) Université de Lorraine, UMR 7359 CNRS Géoresources, 54506 Vandœuvre-lès-
10 Nancy Cedex, France

11 (4) 1 ter rue du Pont, 10450 Bréviandes, France.

12 (5) Agence Nationale pour la gestion des déchets radioactifs, Centre de Meuse/Haute-
13 Marne, RD 960, 55290 Bure, France.

14
15 **Abstract**

16 High-resolution clay mineral analyses were performed on lower and middle Albian
17 deposits from the Paris and Vocontian basins in order to specify the weathering conditions
18 that prevailed at that time. The clay mineral assemblages are composed of small proportions
19 of chlorite and vermiculitic clays associated with abundant illite, R0 type illite-smectite
20 mixed-layers (smectite) and kaolinite. Clay minerals originated from the physical alteration
21 and chemical weathering of rocks and soils outcropping on the Variscan massifs bordering the
22 studied areas. In the Paris Basin, the covariation of illite and kaolinite suggests the reworking
23 of these latter minerals from palaeoalterations and saprolites coupled with an intense runoff
24 on the London-Brabant Massif under a warm-temperate climate.

25 In comparison with the Paris Basin, the lower Albian series deposited in the Vocontian
26 Basin are enriched in smectite because of the preferential deposition of this mineral in deep
27 offshore environments. In this basin, illite and kaolinite did not show any covariation
28 suggesting that kaolinite is rather the chemical weathering product of rocks exposed in the
29 French Massif Central. The stratigraphic distribution of clay minerals in both studied areas is
30 consistent with a cooler and dryer climate around the Aptian/Albian transition. An enhanced
31 precipitation rate is suggested by an increasing proportion of kaolinite from the
32 *Douvilleiceras mammillatum* Zone upward. This humid interval ended in the *Anahoplites*
33 *intermedius* Zone contemporaneous with the smectite-rich sedimentation in the Paris Basin
34 revealing semi-arid conditions consistent with palynological data. This semi-arid interval

35 encompassing the *Dimorphoplites niobe* and *D. biplicatus* zones (and possibly the
36 *Dipoloceras cristatum* Zone) is interrupted at the base of the *Mortoniceras pricei* Zone by a
37 return to a more humid climate.

38

39 Keywords: Clay minerals, Albian, Paris Basin, Vocontian Basin, Palaeoclimate

40

41 **1. Introduction**

42 Most often, the reconstruction of Cretaceous climates is based on an estimate of the
43 ocean surface or deep water temperatures from a variety of proxies including $\delta^{18}\text{O}$, TEX_{86} and
44 more recently Δ_{47} (Friedrich et al., 2012, O'Brien et al., 2017; Meyer et al., 2018). The global
45 climate evolution during the Albian is well known in terms of temperatures inferred from
46 numerous $\delta^{18}\text{O}$ data measured on foraminifera and belemnite guards (Friedrich et al., 2012).
47 After the late Aptian 'coldhouse' climate (Herrle and Mutterlose, 2003; Pirrie et al., 2004;
48 Bodin et al., 2015; Rodríguez-López et al., 2016), the Albian stage is characterized by a
49 regular increase in temperature from the base to the top. This trend continued until the
50 Cretaceous thermal maximum that occurred around the Cenomanian/Turonian boundary
51 (O'Brien et al., 2017; Huber et al., 2018).

52 The estimation of the fluctuations in the hydrological cycle and the intensity of the
53 precipitation during the Albian is discussed much less often (Föllmi, 2012), even though this
54 stratigraphic interval corresponds to dramatic changes in the Earth's history. Albian
55 environments are notably characterized by a radiation of angiosperms and their development
56 in floodplain areas and by the emergence of a narrow humid equatorial climatic belt in
57 comparison with the earlier stages of the Early Cretaceous during which the equatorial humid
58 belt was absent (Chumakov et al., 1995; Poulsen et al., 2001; Chaboureau et al., 2014). A
59 warm and humid belt around the equator is deduced from the common occurrence of bauxite
60 and coal during the Albian (Chumakov et al., 1995). This re-organization of the climatic belts
61 is likely a consequence of the widening of the South and North Atlantic Oceans which thereby
62 introduced a source of moisture (Chaboureau et al., 2014). Therefore, it appears that the
63 Albian was a pivotal period from a climatic point of view that may have had consequences on
64 the hydrological cycle.

65 In the Anglo-Paris Basin, Albian seawater temperatures were estimated using $\delta^{18}\text{O}$
66 analysis of the belemnite guards and fish teeth from the Wissant section outcropping in the
67 Boulonnais area (northwest of the Paris Basin, Bomou et al., 2016, Fig. 1). The measured

68 temperatures on the belemnite guards (bottom waters) range from 13.5 to 19.3°C with an
69 increase from the middle to late Albian. The $\delta^{18}\text{O}$ values for the phosphate in the fish teeth
70 indicate temperatures (from intermediate or sea surface waters) that varied between 22° and
71 28°C with a similar trend. Increasing temperatures during the Albian are consistent with the
72 long-term global warming recorded from the Albian to the Cenomanian using either $\delta^{18}\text{O}$
73 measured in the foraminiferal test or the TEX₈₆ proxy (Friedrich et al., 2012; O'Brien et al.,
74 2017; Kanungo et al., 2018). However, although moisture is a key palaeoclimate parameter,
75 the changes in humidity and weathering conditions that occurred during the Albian are much
76 less documented (Ufnar et al., 2002; Herrle et al., 2003b; Horikx et al., 2017). Our objective is
77 therefore to improve knowledge on humidity/aridity conditions prevailing during the Albian
78 using clay mineral assemblages from sediments deposited in two distinct provinces: the Paris
79 basin (Boreal Province) and the Vocontian basins (Tethyan Province).

80

81 **2. Geological context**

82 During the Albian, the Anglo-Paris Basin was an epicontinental sea connecting the
83 Boreal domain to the north-west and the Tethyan domain to the south-east. It was located at a
84 latitude close to 35°N within a mid-latitude warm humid belt (Fig. 1, Boucot et al., 2013;
85 Amédéo and Matrion, 2014; Gély et al., 2014). The Albian deposits from the type locality
86 (stratotype, department of Aube, south-east of the Paris Basin) were only known by temporary
87 outcrops or quarries where only a few metres of the sedimentary succession can be observed
88 (Amédéo, 1992; Amédéo and Matrion, 2007; 2008, 2014). Consequently, a complete
89 continuous succession could not be established in this part of the Paris Basin. Recently,
90 boreholes were drilled by ANDRA (French agency for nuclear waste disposal) in the
91 department of Aube, allowing the whole lower to middle Albian clayey succession to be
92 examined. The sedimentary series belongs to the so-called 'Argiles tégulines de Courcelles'
93 unit which overlies the Aptian and lowermost Albian greensands, the so-called 'Sables Verts
94 de l'Aube'. In one of the boreholes, the succession encompasses the lowermost part of the
95 overlying 'Marnes de Brienne' of late Albian age.

96 The Paris Basin was bordered to the south-west by the Armorican Massif and the
97 French Massif Central, and to the north-east by the London-Brabant Massif (Fig. 1, Amédéo
98 and Matrion, 2014; Amédéo and Robaszynski, 2014). At that time, north-west Europe was
99 made up of large islands inherited from the Variscan orogeny. Although clay minerals are
100 likely to be deposited very far from their detrital source, the French Massif Central and the
101 London-Brabant Massif were probably the main sources of detrital clay mineral since coeval

102 detrital sandy deposits of the Paris Basin originated from these massifs (Amédro and
103 Robaszynski 2014). These massifs were located at slightly different latitudes and are made up
104 of distinct parent rocks, therefore, significant differences in the composition of clay
105 assemblages can be expected.

106 The Vocontian Basin was located on the northern margin of the Tethys Ocean, around
107 30°N at a somewhat lower palaeoaltitude and closer to the semi-arid belt than the Paris Basin
108 (Chumakov et al., 1995, Hay and Floegel, 2012; Fig. 1). This basin was surrounded by
109 shallow platforms except to the east where it was largely opened to the Tethys Ocean (Fig. 1).
110 Lower to middle Albian deposits (Blue Marls Formation) are well-exposed in several sections
111 (Bréhéret, 1997; Gale et al., 2011). The Col de Pré-Guittard section was chosen for this study
112 considering its location in the western part of the Vocontian Basin, far from thermal
113 influences that would transform detrital clay minerals. This reference section is also clearly
114 defined with biostratigraphy (Kennedy et al., 2000, 2014; Petrizzo et al., 2012), and was
115 approved recently as the Albian Global Boundary Stratotype Section and Point (GSSP)
116 (Kennedy et al., 2017).

117

118 **3. Lithology and biostratigraphy**

119 **3.1. Boreholes from the Paris Basin**

120 Two boreholes (AUB111 and AUB220) located close to Juzanvigny, and one borehole
121 drilled close to Vallentigny (AUB240) were studied (Fig. 2). Samples were taken every meter
122 in the borehole AUB240 and every 50 centimeters in the boreholes AUB111 and AUB220.

123 The distance between boreholes AUB111 and AUB220 is only 1 km. One of the cores
124 (AUB111, Fig. 3) has been described in detail including a precise biostratigraphic scheme on
125 the basis of the abundant ammonite fauna (Amédro et al., 2017) following the ammonite
126 biozonation proposed by Amédro and Matrion (2014). Lower to middle Albian deposits
127 (Argiles tégulines de Courcelles) essentially consist of bioturbated clays and silty clays with
128 occasional pyrite and phosphate nodules (Knight 1999). Phosphate nodules are either
129 scattered or in the form of thin horizons that may be correlated at a regional scale. The base of
130 the unit is more or less sandy, with increasingly more abundant glauconite further down the
131 core, until the boundary with the Aptian greensands (Sables Verts de l'Aube Formation).
132 Borehole AUB 220 shows a sedimentary succession quite similar to that described in borehole
133 AUB111, but it can be used to provide more descriptions further upward in the series (Figs. 4
134 and 5; Supplementary Appendix). In addition, the recovery across the boundary between the
135 Sables Verts de l'Aube and the Argiles tégulines de Courcelles is better than in the AUB111

136 borehole. Notably, a condensed horizon composed of a 10 cm-thick phosphatic crust
137 corresponding to a hardground is particularly well preserved in this borehole (Fig. 5). The age
138 of the deposits recovered in the lower part of the two boreholes is not well established. In this
139 part of the Paris Basin, the Sables Verts de l'Aube unit is considered to be Aptian in age
140 (Amédro and Matrimon 2007) because of the occurrence of the benthic foraminifera
141 *Verneuilinoides subfiliformis* which suggests that the Sables verts de l'Aube belong to the
142 *Hypacanthoplites jacobi* Zone from the upper Aptian (Damotte & Magniez-Jannin, 1973;
143 Mutterlose et al., 2003).

144
145 The phosphatic crust corresponds to a condensed interval that, according to previous
146 studies on outcrops located in the same region, likely includes the *Leymeriella tardefurcata*
147 and *Leymeriella regularis* ammonite zones (Amédro and Matrimon 2007, 2014). At the base of
148 the two boreholes, the 5 m-thick interval between the phosphatic crust and the first occurrence
149 of *D. mammillatum* is not well dated as only *Beudanticeras* sp. have been found. This interval
150 probably successively corresponds to the *Sonneratia kitchini*, *Cleonicerias floridum* and
151 *Hemisonneratia puzosiana* zones compared with the sections outcropping to the south-east of
152 the Paris Basin (Destombes in Rat et al., 1979; Amédro et al., 2000; Amédro and Matrimon,
153 2008). Above this poorly dated interval, the borehole is precisely dated by numerous
154 ammonites which can be used to draw an accurate biostratigraphic scheme (Figs. 3-5). The
155 two boreholes can be easily correlated in particular by using marker beds that include
156 horizons of phosphate nodules and bio-events (Amédro et al., 2019).

157 The change from the Aptian greensands, deposited in shoreface, estuarine or fluvio-
158 deltaic environments (Guillocheau et al., 2000), to the Argiles tégulines de Courcelles
159 deposited in offshore environments clearly indicates a deepening of the depositional
160 environments as a consequence of the early Albian transgression from the south-west through
161 the Burgundy high (Pictet et al., 2018). This transgressive trend is also expressed by the
162 occurrence of cosmopolitan ammonites indicating the opening of the Burgundy threshold
163 (Fig. 1).

164 The third borehole, AUB240 (Fig. 2), shows a similar lithological succession but the
165 upper part of the borehole has permitted the recovery of the topmost part of the Argiles
166 tégulines de Courcelles and the lowermost part of the Marnes de Brienne (Fig. 7). The
167 recognition of marker beds between the three boreholes allows precise correlations to be
168 drawn (Amédro et al., 2019). In the upper part of this borehole, all ammonite zones were

169 recognized except the *Dipoloceras cristatum* Zone which is condensed and corresponds to the
170 occurrence of a phosphate nodule bed (Amédro et al., 2019).

171

172 3.2. The Col de Pré-Guittard section (Vocontian Basin)

173 The Col de Pré-Guittard section (Fig. 8) shows the lower to middle Albian
174 sedimentary succession, which is part of the Blue Marls Formation. It mainly consists of
175 hemipelagic blue-grey marls punctuated by several marker beds and bundles of micritic
176 limestones used as marker horizons to refine the correlations throughout the basin (Friès,
177 1987; Bréhéret, 1997). Organic matter-rich layers (black shales) are also common, the most
178 prominent of these being the Paquier horizon corresponding to the sedimentary expression of
179 Oceanic Anoxic Event (OAE) 1b (Bréhéret, 1985 a and b; Tribovillard and Gorin, 1991; Hart
180 et al., 1996; Erbacher et al., 1999; Herrle et al., 2003b). The section has been measured from
181 the Aptian/Albian transition (Kilian bundle) to the lowermost middle Albian. Samples were
182 taken every metre.

183 Because different ammonite biozonations (Boreal vs Tethyan) are used in sections from the
184 Paris Basin and the Vocontian Basin, correlations are difficult, however a comparison
185 between the ammonite biozones used in both study areas is given in Table 1. Notably, the *D.*
186 *mammillatum* Zone used in the Vocontian Basin includes the *S. kitchini*, *C. floridum*, *H.*
187 *puzosiana*, *Otohoplites subhilli* and *Hoplites (Isohoplites) steinmanni* zones. During the
188 Albian, the Paris Basin belonged to the Northern European Faunal Province of the Boreal
189 Domain, characterized by the presence of rich populations of Hoplitidae that followed each
190 other (including genera *Sonneratia*, *Hemisonneratia*, *Otohoplites*, *Hoplites*, *Anahoplites*, and
191 *Dimorphoplites*), allowing the definition of many biozones. The Vocontian Basin, located on
192 the northern margin of the Tethyan Domain, contains more occasional and less diversified
193 faunas at the top of the lower Albian and in the middle Albian (*Douvilleiceras*, then
194 *Lyelliceras* and *Oxytropidoceras*). At the top of the lower Albian, the correlation between the
195 two basins is based on the vertical distribution of the species *Douvilleiceras mammillatum*
196 which appears just above the *L. regularis* Zone and disappears at the top of the *Lyelliceras*
197 *lyelli* Zone (or Subzone). In the middle Albian, *Oxytropidoceras roissyanum* is known at Col
198 de Palluel at the top of this Substage (Gale et al., 2011), but here, the absence of ammonite in
199 the lower levels does not allow to recognise the total vertical distribution of this species. The
200 appearance of *O. roissyanum* is however well documented both in northern France (Amédro,
201 2009) and Kent in south-east England (Young et al., 2010), from the *Hoplites dentatus* Zone.
202 Therefore, the *O. roissyanum* Total Range Zone used in this paper comprises successively the

203 *Hoplites dentatus*, *Anahoplites intermedius*, *Dimorphoplites niobe* and *D. biplicatus* zones in
204 the Anglo-Paris Basin.

205

206 **4. Methods**

207 4.1. Mineralogy

208 A total of 400 samples were analysed using X-Ray Diffraction (XRD). After moderate
209 grinding in a mortar, powdered samples were decarbonated with a 0.2N HCl solution. The
210 < 2 µm fraction (clay-sized particles) was extracted with a syringe after decantation of the
211 suspension for 95 minutes following Stokes' law; this fraction was then centrifuged. Clay
212 residue was then smeared on oriented glass slides and run in a Bruker D4 Endeavour
213 diffractometer with CuK α radiations, a LynxEye detector and a Ni filter with a voltage of 40
214 kV voltage and an intensity of 25 mA (Biogéosciences laboratory, University of Burgundy,
215 France). Goniometer scanning ranged from 2.5° to 28° for each analysis. Three runs were
216 performed for each sample to discriminate the clay phases: 1) air-drying; 2) ethylene-glycol
217 solvation; and 3) heating at 490°C, as recommended by Moore and Reynolds (1997) (Fig. 9).
218 Clay minerals were identified using their main diffraction (d₀₀₁) peak and by comparing the
219 three diffractograms obtained. The following main clay minerals were identified (Fig. 9) : a
220 R0 type illite-smectite mixed-layer (17 Å based on a glycolated run condition) referred to as
221 smectite for the following sections; a R1 type illite-smectite mixed-layer (around 11.5 Å in
222 air-drying conditions and 13 Å after ethylene-glycol solvation); chlorite (14.2 Å, 7.1 Å, 4.7 Å
223 and 3.54 Å peaks); illite (10 Å, 5 Å, 3.33 Å peaks); kaolinite (7.18 Å and 3.58 Å peaks) and
224 vermiculitic clays including true vermiculite (14 Å in air-drying conditions, 14.5-15 Å after
225 ethylene-glycol solvation and 10 Å peaks after heating) and chlorite-vermiculite mixed-layers.
226 The relative proportions of clay minerals are estimated using peak intensity ratios, the most
227 relevant of these being the ratio between the 7.18 Å and 17 Å peaks corresponding to
228 kaolinite + chlorite/smectite (K+C/S). The error of this method is approximately ± 5 %.
229 This ratio can be taken as an estimate of the humidity vs aridity.

230 Fifteen samples have been measured for CaCO₃ content on the AUB 111 borehole
231 with a Bernard's calcimeter device (uncertainty of ~1%). No measurement were done in the
232 Vocontian Basin as Bréhéret, (1997), previously performed it. We only compared the GRS
233 signal that we measured on the field with the CaCO₃ content given by Bréhéret (1997).

234

235 4.2 Spectral gamma ray (SGR)

236 SGR measurements were taken on the Col de Pré-Guittard section every 50 cm at the
237 same position as for the samples collected for XRD. Field SGR measurements were taken
238 with a constant 1-min acquisition time using a Geofyzica-Statist-Geo GS-512 spectrometer
239 with a Cesium 137 scintillation detector. For all readings, the detector was placed against
240 outcrop surfaces that had been cleaned of weathered material and smoothed. A scintillometer
241 arrangement was used to produce an energy spectrum for the natural gamma rays emitted
242 from an outcrop. This spectrum was interpreted electronically to yield concentrations of the
243 principal gamma ray sources involved, namely potassium (K), thorium (Th) and uranium (U).
244 K and Th are usually concentrated in clay minerals whereas U is associated with organic
245 matter (Myers and Wignall, 1987). SGR values are given in ppm (eq. U). Measurement
246 reproducibility is assessed at 5% (1σ) by repeating the same measurement 30 times (Martinez
247 et al. 2013). The spectral gamma ray is an effective tool for the preliminary assessment of the
248 degrees of palaeoweathering (clay content) and is therefore commonly used for palaeoclimate
249 reconstructions (Ruffell et al., 2016).

250

251 **5. Results**

252 5.1. Paris Basin

253 In the Argiles tégulines de Courcelles unit, the CaCO_3 proportions are between 10%
254 and 15% except in some marly limestones where the CaCO_3 content reaches 40%. Smear
255 slides performed on some clayey samples show abundant nannofossils which are likely
256 responsible for the CaCO_3 content. Consequently, clay minerals represent a significant
257 amount of the deposits.

258

259 *Clay mineralogy*

260 The clay mineral assemblages of the AUB111 borehole are mainly composed of illite
261 (28% on average), vermiculitic clays (10% on average), smectite (22% on average) and
262 kaolinite (26% on average). They also contain chlorite ($\leq 5\%$), R1 type illite-smectite mixed-
263 layers and chlorite-vermiculite mixed-layers, which are both estimated to be 5% or less (Fig.
264 3). The composition of the mineralogical assemblages along the borehole allows to
265 distinguish three different intervals. At the base of the borehole, from 69.10 to 63.96 m, the
266 first poorly-dated interval is characterized by abundant smectite (up to 70%), illite, and very
267 low proportions of kaolinite. Some illite-rich samples occur in the glauconitic interval, close
268 to the transition with the greensands. The presence of glauconite in the deposits is confirmed
269 by the observation of smear slides. Above, the second interval is marked from 63.96 to 13.35

270 m by increasing proportions of kaolinite and illite together with vermiculitic clays in
271 significant proportions (up to 15%), while the smectite proportion decreases. In this interval,
272 the proportions of illite generally range between 20 and 30%, with occasionally more
273 abundant proportions reaching 40% (Fig. 3). The disappearance of vermiculitic clays and the
274 higher proportions of smectite (~ 40%) characterize the third interval, above 13.35 m while
275 the percentages of kaolinite and illite decrease. The transition from the second to the third
276 interval occurs around the transition from the *A. intermedius* to *D. niobe* ammonite zones.

277 The clay mineralogy of the AUB220 borehole is quite similar to that described in
278 AUB111 indicating that the clay mineralogy of the Argiles Tégulines de Courcelles is, as
279 expected, homogeneous at a kilometer scale (Figs. 4 and 5). The increase in smectites content
280 in the third interval is better expressed, since this borehole includes an upper part of the
281 Argiles tégulines de Courcelles (Figs. 4 and 5).

282 In the upper part of borehole AUB240, a fourth interval is observed from 8.75 to 27.3
283 m marked by a decrease in smectite while increasing proportions of illite, vermiculitic clays
284 and kaolinite are observed in the *pricei* Zone (Fig. 7). Therefore, within the Argiles tégulines
285 de Courcelles, the *D. niobe/D. biplicatus* time-equivalent interval is characterized by a
286 smectite-rich sedimentation compared to the rest of the formation. This evolution in the clay
287 assemblages confirms the low-resolution clay mineral data published by Fauconnier (1975)
288 and Pomerol (1986).

289

290 5.2. Vocontian Basin

291 The clay mineral assemblages of the Col de Pré-Guittard section are mainly composed
292 of smectite (63% on average), illite (19% on average) and kaolinite (11% on average). They
293 also contain about 5% of chlorite (Fig. 10). Traces of R1 type illite-smectite mixed-layers and
294 chlorite-vermiculite mixed-layers may be present ($\leq 2\%$) in some samples and although they
295 were taken into account in the calculation, they are not represented in Figure 10. The clay
296 composition is marked by a gradual smectite decrease from 70% from the base to 60% at the
297 top of the section. This decrease corresponds to a clear increase in kaolinite with values in the
298 order of 5% down section to values greater than 15% above. Interestingly, as in the Paris
299 Basin, sedimentary rocks located around the Aptian/Albian boundary are depleted in
300 kaolinite. The proportion of kaolinite increases during the *L. tardefurcata* ammonite Zone but
301 remains generally below 10%, while in the *D. mammillatum* Zone, the proportions of
302 kaolinite are higher than 10%.

303 According to Br  h  ret (1997), the CaCO₃ content is approximately 20% at the base of
304 the section and increases to approximately 40% at the top, which is consistent with our SGR
305 measurements that show a reverse long-term trend with decreasing values from the base to the
306 top of the section (Fig. 10). This expected inverse relationship between the SGR
307 measurements and the CaCO₃ content was already observed in the Aptian part of the Blue
308 Marls Formation (Ghirardi et al., 2014).

309

310 **6. Discussion**

311 6.1. Influence of burial diagenesis

312 Burial diagenesis may transform clay mineral assemblages leading to a misreading of
313 the original paleoclimatic and paleoenvironmental signal. Before examining the
314 environmental significance of the clay minerals, it is important to ensure that they are
315 dominantly detrital without any significant influence of burial diagenesis.

316 In the Paris Basin, the post-Albian geological history includes the deposition of the
317 Upper Cretaceous chalk, the maximum thickness of which probably never exceeded 1000 m.
318 At least 700 m of the Cenomanian to lower Campanian chalk was preserved in the depocentre
319 of the Paris Basin (Robaszynski et al., 2005) but the total thickness was greater since the
320 upper Campanian to Maastrichtian chalks have been dissolved (the Maastrichtian chalk is
321 known as reworked pebbles) and eroded during the latest Cretaceous. Consequently, the
322 Upper Cretaceous chalk is separated from the Cenozoic deposits by a major unconformity
323 truncating Late Cretaceous folds (Guillocheau et al., 2000). In the eastern part of the Paris
324 Basin, the chalk series was probably thinner but this was difficult to evaluate. Detailed
325 reconstructions of the thermal evolution of the eastern part of the Paris Basin indicate that
326 even in the Late Jurassic, the maximum burial temperature reached by the end of the
327 Cretaceous never exceeded 50-60  C (Pellenard et al., 1999; Blaise et al., 2014; Mangenot et
328 al., 2018). Consequently, in the overlying Albian deposits, the temperature remained low; this
329 is confirmed by the abundance of smectite, as these minerals are known to be particularly
330 sensitive to burial diagenesis and are transformed into R1 illite-smectite mixed-layers and
331 illite through illitization processes at temperatures over 60-70  C (Merriman and Frey, 1999;
332 Lanson et al., 2009;   rodo  n et al., 2009; Dellisanti et al., 2010). As a result, the abundance of
333 smectite from the lowermost part of the studied boreholes indicates that the temperatures
334 never exceeded 60-70  C and that the clay minerals are mostly primary and detrital in origin.

335 In the Vocontian Basin, for the same reasons, the abundance of smectite indicates a
336 negligible influence of burial diagenesis on the clay mineralogy. Numerous studies have

337 shown that in the western part of the Vocontian Basin, the influence of diagenesis on clay
338 minerals from Lower Cretaceous formations is weak (Deconinck and Chamley, 1983; Ferry et
339 al., 1983; Deconinck and Debrabant, 1985, Levert and Ferry, 1988). In the Col de Pré-
340 Guittard section, Rock-Eval analyses performed on organic matter-rich horizons show that
341 T_{\max} values are comprised between 417 and 437°C indicating that organic matter is immature
342 or at the onset of the oil window, thereby confirming that the influence of thermal diagenesis
343 remained weak on this section (Bréhéret, 1997).

344

345 6.2. Authigenic clay minerals

346 Detrital clay assemblages may be modified by the authigenesis of clay minerals
347 formed either during early or late successive diagenetic steps. Authigenic glauconite (iron-
348 rich illite) is common in Albian deposits notably at the transition between the greensands and
349 the Argiles tégulines de Courcelles that is at the base of the boreholes studied in the Paris
350 Basin. Although glauconite granules are much coarser than the clay fraction, after grinding
351 the samples, glauconitic illite is inevitably partly incorporated in the clay fraction and could
352 be responsible for some abnormally high proportions of illite thus corresponding to a mixture
353 of detrital and authigenic minerals (Fig. 3). This likely occurs at the base of the boreholes at
354 the transition between the Sables verts de l'Aube and the Argiles tégulines de Courcelles.

355 A detailed study of clay minerals from similar Albian deposits (Gault clay) from the
356 Wissant section in the Boulonnais area (Northwest of the Paris basin) shows that the clay
357 fraction includes two types of smectites corresponding to beidellite (dioctahedral Al-Fe
358 smectite). The first type, showing a fleecy shape under transmission electron microscope
359 (TEM), is considered to be detrital, while the second displays a lathed shape due to the
360 development of crystalline overgrowths indicating authigenesis (Holtzapffel, 1985; Steinberg
361 et al., 1987). It is hypothesized that crystalline overgrowths are the result of an early
362 diagenetic recrystallization of detrital smectites and may represent an early stage of
363 glauconitization. Lath-shaped smectites are widespread in Meso-Cenozoic deposits
364 (Holtzapffel et al., 1985; Deconinck and Chamley, 1995) and result from
365 dissolution/recrystallization processes in relatively closed environments (Clauer et al., 1990).
366 However, the development of this type of authigenic minerals does not seem to significantly
367 modify the composition of the detrital clay fractions.

368 In both studied areas, we therefore consider that the clay minerals are mainly detrital
369 and originated from the erosion of nearby emerged lands, knowing that 1) glauconitic illite
370 may be associated with detrital illite, notably in the Paris Basin at the transition between the

371 Sables Verts de l'Aube and the Argiles tégulines de Courcelles and 2) authigenic smectite
372 may have marginally enhanced the total proportion of smectites in specific closed
373 environments.

374

375 6.3 Origin of clay minerals

376

377 Although clay particles may be transported over long distances (Chamley, 1989),
378 during the Albian, a large part of the clay minerals potentially originated from the landmasses
379 composed of the French Massif Central and the Armorican massifs, and from the London-
380 Brabant Massif which were the main emerged lands around the studied areas (Fig. 1). Clay
381 minerals were likely transported to the sea mainly by rivers and then deposited by decantation
382 relatively far from the shoreline. In the Paris basin, the erosion of the two massifs probably
383 fed the sedimentation, whereas the clays from the Vocontian Basin had to come from the
384 basement and the sedimentary cover of the French Massif Central and other emerged lands
385 located to the south (Corso-Sarde microcontinent?, Fig. 1).

386 The lithology of the London-Brabant Massif and the French Massif Central is
387 different. These massifs are both inherited from the Variscan orogeny, but magmatic and
388 high-grade metamorphic rocks (granitoids, migmatites, and gneiss) are predominant in the
389 French Massif Central, whereas low-grade metamorphic and sedimentary rocks dominated in
390 the London-Brabant Massif (schists, slates, limestones and shales; Fielitz and Mansy, 1999;
391 Han et al., 2000). Therefore, a different nature can be expected from the contributions of clay
392 minerals originating from these two massifs. In addition, they were not located at the same
393 latitudes, and according to the estimated precipitation rates during the 'Mid-Cretaceous'
394 (Ufnar et al., 2002; 2004), the French Massif Central was located between 25 and 30°N close
395 to an arid to semi-arid climatic belt extending southward toward Portugal and West Africa
396 (Fenner, 2001; Heimhofer et al., 2008), while the London-Brabant Massif was located
397 between 30 and 35°N in a more humid tropical belt.

398

399

400 6.3.1. Primary clay minerals

401 Primary clay minerals, i.e. chlorite and illite, are mainly formed through weathering
402 processes of metamorphic and igneous rocks yet these minerals can be also reworked from a
403 sedimentary basement (Chamley, 1989; Weaver 1989). In Albian deposits, chlorite never
404 exceeds 5% of the clay fraction which is common in Cretaceous sedimentary rocks that have

405 not undergone a deep burial (Deconinck et al., 1985; Kühn et al., 2001). The scarcity of
406 chlorite is explained by the overall warm and humid climate that prevailed at that time, as
407 chlorite is easily weathered under such climate conditions (Deconinck et al., 1985). Illite
408 primarily characterizes the mechanical erosion of a mica-rich crystalline basement (notably
409 muscovite). The common occurrence of significant amounts of this mineral is explained by its
410 reworking from the Variscan igneous and metamorphic massifs. The higher illite abundance
411 in the Paris Basin (close to 30%) than in the Vocontian Basin (close to 20%) likely results
412 from the differential settling processes of clay minerals: illite is preferentially deposited
413 nearshore whereas smectites, because of their better buoyancy, are exported further out in the
414 ocean (Gibbs, 1977; Chamley, 1989). This difference is then explained by the distinct
415 palaeogeographical context of the two sedimentary basins, as the Col de Pré-Guittard
416 Formation was likely in a more distal position compared with the emerged lands than the
417 boreholes located in the eastern part of the Paris Basin.

418 6.3.2. Origin of kaolinite

419 There are two possible origins of kaolinite in the deposits. Kaolinite may originate
420 from soils where it accumulated due to the partial hydrolysis of silicates including feldspars
421 and other minerals which can be easily weathered (Chamley, 1989); it is subsequently
422 transported and integrated into marine sediments. Kaolinite may be also reworked from older
423 kaolinite-bearing sedimentary rocks or palaeoalterations (Deconinck and Vanderaveroot,
424 1996; Thiry, 2000). In the first case, kaolinite is indicative of a warm and humid climate
425 responsible for strong hydrolysis, whereas in the second case, kaolinite is only indicative of a
426 significant runoff on the continents. In both cases, the occurrence of kaolinite indicates a
427 humid climate (Chamley, 1989; Ruffell et al., 2002; Dera et al., 2009; Bougeault et al., 2017).
428 However, when kaolinite is reworked from ancient rocks, it can be expected to observe a
429 covariation with illite as this mineral results from the same process, whereas when kaolinite
430 originates from soils, its evolution through time should be decoupled from that of illite.

431 A clear covariation of illite and kaolinite is observed in the Paris Basin, suggesting
432 that kaolinite is dominantly reworked from kaolinite-bearing rocks and palaeoalterations
433 rather than from soils formed at the time of sedimentation. After the Purbeckian (latest
434 Jurassic/earliest Cretaceous) regressive facies (Brigaud et al., 2018), the Paris Basin
435 corresponded to a continental area where early Cretaceous Wealden facies accumulated. At
436 that time, the surrounding massifs, remnants of the Variscan orogeny, were deeply weathered
437 with the formation of kaolinite-rich soils, saprolites and bauxites over the French Massif

438 Central, the London-Brabant Massif and the Armorican Massif (Thiry et al., 2005). Apatite
439 fission-track thermochronology performed on the Ardennes Massif suggests that the
440 sedimentary cover of the London-Brabant Massif was eroded during the Late Jurassic and
441 Early Cretaceous (Barbarand et al., 2018). A major alteration phase favoured by a tectonic
442 rejuvenation in the southern part of the London-Brabant Massif took place during the Early
443 Cretaceous and then this massif underwent a kaolinitic alteration (Quesnel, 2003; Yans, 2003;
444 Thiry et al., 2005; 2006). In agreement with the Mid-Cretaceous study of the Isle of Wight
445 (Gale et al., 1996; Ruffell and Garden, 1997), we suggest that clay minerals from the Albian
446 deposits of the Anglo-Paris Basin preferentially originated from the north (i.e. the London-
447 Brabant Massif). However, Lower Cretaceous bauxitic profiles have also been identified in
448 the French Massif Central (Thiry et al., 2005), which could constitute an additional source of
449 reworked kaolinite. Therefore, the high proportions of kaolinite in the Albian deposits of the
450 Paris Basin could be explained by the erosion of the kaolinite-rich weathering profile
451 developed over the Variscan massifs during the Early Cretaceous. As detrital clays including
452 kaolinite may be reworked from older rocks or from palaeoalterations, their climatic
453 significance may be questioned (Jeans et al., 2001), but overall, the illite and kaolinite
454 dominated clay assemblages of the Albian in the Paris Basin point to a significant runoff and
455 consequently humid climate conditions.

456 In the Vocontian Basin, kaolinite proportions increase slightly from the base to the top
457 of the section, whereas the proportions of illite remain stable. This suggests that kaolinite and
458 illite deposited in the Vocontian Basin primarily originated from distinct sources. Illite likely
459 originated from the crystalline basement whereas kaolinite was probably at least partly
460 derived from soils or palaeoweathering profiles developed over the French Massif Central or
461 other further away areas. These mineralogical features suggest slightly increasing humidity
462 during the early Albian.

463 6.3.3. Origin of smectite

464 Smectites seem predominantly detrital, whether in the Albian in the Boulonnais area
465 or southern England (Holtzapffel, 1985; 1987; Gale et al., 1996). Their Al-Fe beidellite
466 composition suggests a reworking from soils developed on the Variscan massifs under a warm
467 and seasonally humid climate (Chamley, 1989). These minerals are abundant in a poorly-
468 dated interval likely corresponding to the *L. tardefurcata/L. regularis* ammonite Zone in the
469 lowermost part of the Argile tégulines de Courcelles (Figs. 3-5). Smectites are also abundant
470 in the uppermost middle Albian corresponding to the *D. niobe* and *D. biplicatus* ammonite

471 zones (Figs. 3-5, and 7). During these intervals, smectite-rich sedimentation suggests that the
472 semi-arid climatic belt expanded northward.

473

474 6.3.4. Origin of vermiculitic clays

475

476 In the Paris Basin, the Argiles tégulines de Courcelles contain significant amounts of
477 vermiculitic clays, in association with illite and kaolinite whereas these minerals are almost
478 absent from the Vocontian Basin. These clay minerals are relatively unusual in Mesozoic
479 marine sedimentary rocks, although vermiculite is also mentioned in coeval middle Albian
480 deposits (Gault Clay) from the Isle of Wight in England (Gale et al., 1996). Therefore,
481 vermiculitic minerals are likely deriving together with illite and kaolinite from a source that
482 could possibly be the London-Brabant Massif (Fig. 11A). This mineral may originated from
483 soils formed under cold-temperate climate (Li et al., 2019), but such climatic conditions seem
484 unlikely at relatively low latitudes during the Albian. We therefore suggest that vermiculitic
485 clays are reworked from the basement (moderate weathering of chlorite) or from
486 palaeoalterations.

487

488 6.4. Environmental controls of the early/middle Albian clay sedimentation

489 The mineralogical composition of the clay assemblages is the result of a complex
490 interplay of the lithology of the emerged landmasses, their reliefs and tectonic instability, sea-
491 level fluctuations and climate (e.g., Chamley, 1989).

492 In the Paris Basin, clay sedimentation largely dominated by illite and kaolinite
493 suggests that the London-Brabant Massif was submitted to significant runoff conditions.
494 Between 30 and 35°N, corresponding to the palaeolatitudes of the London-Brabant Massif,
495 precipitation rates are estimated between 1000 and 1500 mm/yr (Ufnar et al., 2002), which is
496 high enough to produce erosional soil processes, the erosion of Lower Cretaceous kaolinite-
497 rich palaeoalterations and the bedrock. These conditions were probably responsible for a
498 significant detrital flux of clay minerals such as illite and kaolinite (Fig. 11). As the
499 temperatures were also high (>20°C for these palaeolatitudes, based on $\delta^{18}\text{O}$ values; O'Brien
500 et al., 2017), chlorite was likely rapidly transformed into vermiculite and interstratified
501 minerals including chlorite-vermiculite which are identified in small quantities in the Albian
502 sedimentary rocks (Herbillon and Makumbi, 1975; Proust et al., 1986; Righi et al., 1993;
503 Banfield and Murakami, 1998).

504 The two smectite-rich intervals identified in the Albian of the Paris Basin, the first one
505 close to the Aptian/Albian transition and in the lowermost Albian and the second from the *A.*
506 *intermedius* to the *D. biplicatus* ammonite zones in the lower middle Albian, clearly indicate
507 that the erosional processes were less intense. A decreasing intensity of erosion may be linked
508 to rising sea level or to a shift from humid to more arid conditions. At the base of the
509 succession in the lower Albian, the long-term transgressive trend may be responsible for the
510 smectite-rich sedimentation, but this trend lasted during the entire Albian (Haq, 2014) while
511 abundant illite and kaolinite replaced the smectite-rich sedimentation. The comparison of clay
512 assemblages with short-term sea level curves (Haq, 2014) did not show any relationship
513 between clay assemblages and sea level fluctuation. In addition, in the study area, the time-
514 equivalent interval for the *D. niobe* and *D. biplicatus* zones is known to correspond to a low
515 relative sea level (Amédéo and Matrimon, 2014). Consequently, smectite-rich sedimentation
516 does not seem to be the result of a rising sea level. However, these particular intervals,
517 previously identified in the Boulonnais area (Holtzapffel 1985; 1987) and in southern England
518 (Isle of Wight, Gale et al., 1996) can be explained by more arid climate conditions. As the
519 Aptian-Albian transition is known to be a cool interval (Millán et al., 2014 and references
520 therein), the hydrological cycle was probably slower during this period which is consistent
521 with dryer conditions reflected by smectite-rich sedimentation intervals. Such climate
522 conditions are also suggested in southern Portugal (Algarve) where mineralogical and
523 palynological data indicate more aridity (Heimhofer et al., 2008). The smectite-rich
524 sedimentation in the upper part of the middle Albian (*A. intermedius* to *D. biplicatus* zones)
525 may be also explained by a semi-arid climate and a cooling trend suggested by calcareous
526 nannofossils and the isotope chemistry of the Gault Clay from south-eastern England
527 (Kanungo et al., 2018). Such climate conditions are also known in northern Spain before more
528 humid conditions occurred during the late Albian (Sender, 2005; Coiffard et al., 2007). In the
529 Lusitanian Basin, in the time-equivalent interval, coupled palynological and clay mineral data
530 indicate drier conditions characterized by the abundance of *Classopollis* and by decreasing
531 proportions of kaolinite balanced by increasing proportions of illite-smectite mixed-layers
532 (Heimhofer et al., 2012).

533 In the Vocontian Basin, the Aptian/Albian transition is also characterized by kaolinite-
534 depleted deposits which is consistent with drier conditions (Fig. 11B). The proportions of this
535 mineral slightly increased during the *L. tardefurcata* ammonite Zone but stayed relatively
536 low. A significant increase occurs in the *D. mammillatum* Zone, partly time equivalent to the

537 *O. subhilli* and *H. steinmanni* zones from the Paris Basin, which represents the upper half of
538 the *D. mammillatum* Zone (see Table 1 and Fig. 11B). This trend is comparable with the
539 increase of kaolinite recorded in the Paris Basin (Fig. 11B) and likely reflects wetter climatic
540 conditions as a consequence of the emergence of a humid equatorial belt during the Albian
541 (Chumakov et al., 1995). There may be several possible explanations for the significant
542 difference between the percentages of kaolinite in the Paris Basin (between 25 and 30%) and
543 Vocontian Basin (between 10 and 15%). It is well-known that differential settling processes
544 of clay minerals favour the nearshore deposition of kaolinite whereas smectite, because of its
545 better buoyancy, is deposited further out in the ocean (Deconinck et al., 1985; Godet al.,
546 2008). In addition, clay minerals deposited in the Vocontian Basin may originated from
547 distinct detrital sources, some of which are located southward (Corso-sarde micro-continent?)
548 in the semi-arid climatic belt where smectite should form in soils.

549 Surprisingly, clay assemblages do not display any particularity in the stratigraphic interval
550 encompassing the organic matter-rich Paquier horizon (OAE1b) in the Col de Pre-Guittard
551 section. However, the K+C/S ratio increases slightly around this level. Most works show that
552 the temperature increased sharply during this event and some authors suggest that the
553 monsoonal climate enhanced the humidity and detrital supply during this peculiar event
554 (Herrle et al., 2003a and b; Hofmann et al., 2008; Jenkyns, 2010; Sabatino et al., 2015), which
555 is consistent with our clay mineralogical results.

556 In the Paris Basin, the upper Albian deposits (*pricei* Zone) again show a kaolinite- and
557 illite-rich clay fraction (Fig. 6) indicating a return to more humid climate conditions. The base
558 of the late Albian is characterized by a warm event recorded during the *D. cristatum* Zone
559 (Kanungo et al., 2018). Unfortunately, this stratigraphic interval is condensed in the boreholes
560 studied here, but the above mentioned warming event (Kanungo et al., 2018) may be
561 responsible for an accelerated hydrological cycle and consequently enhanced erosional
562 processes on the London-Brabant Massif during the overlying *M. pricei* Zone. Alternatively,
563 the tectonic instability of the London-Brabant Massif during the early late Albian (Owen,
564 1971) could be also responsible for the concomitant increase in illite and kaolinite.

565

566 **Conclusions**

567 The clay mineralogy of the Albian deposits in the Paris and Vocontian basins shows
568 some common features suggesting at least a regional climatic control of the clay
569 sedimentation as well as specific characteristics attributable to certain local conditions.

570 The kaolinite-depleted interval around the Aptian/Albian transition and in the
571 lowermost Albian suggests that a relatively cool and dry climate was likely responsible for a
572 slow-down of the hydrological cycle. From the *D. mammillatum* Zone in the Vocontian Basin
573 and at least from the *H. puzosiana* to the *A. intermedius* Zone in the Paris Basin, increasing
574 proportions of kaolinite and/or illite suggest increased precipitation rates and a more constant
575 humid climate. This change may be the consequence of the re-organization of the climatic
576 belts, particularly the emergence of the equatorial humid zone favouring a warm humid belt at
577 latitudes between 25 and 35°N. In the Paris Basin, kaolinite is primarily reworked from
578 Lower Cretaceous palaeoalterations and from unmetamorphosed rocks outcropping on the
579 London-Brabant Massif, whereas in the Vocontian Basin, this mineral may be also reworked
580 from soils developed over the Central Massif and other continental masses located
581 southwards. In both cases, increasing proportions of kaolinite are indicative of increased
582 runoff triggered by a more humid climate and a southward shift of the mid-latitude warm
583 humid belt.

584 During the late-middle Albian (at least in the *D. niobe* and *D. biplicatus* ammonite
585 zones), the smectite-rich sedimentation in the Paris Basin suggests a latitudinal expansion of
586 the semi-arid climatic belt which is consistent with palaeobotanical data. During the late
587 Albian (*M. pricei* Zone), illite and kaolinite contents increase again indicating either a return
588 to a more humid climate and/or the influence of a tectonic instability of the London-Brabant
589 Massif.

590 The occurrence of vermiculitic clays restricted to the Anglo-Paris Basin suggests that
591 this mineral originated from the London-Brabant Massif. Finally, the smectite-rich
592 sedimentation recorded in the Vocontian Basin compared with the Paris Basin illustrates the
593 significant role played by the differential settling of clay minerals from nearshore to offshore
594 environments and by palaeogeography.

595 Finally, the warm climates of the Albian also seem to be characterized by fluctuations
596 in humidity with significant impacts on the continental weathering processes.

597

598 **Acknowledgements**

599 We would like to thank Claude Aurière, who is in charge of Andra's core storage, for his help
600 in studying the boreholes. Alexis Godet and an anonymous reviewer are also gratefully
601 acknowledged for their constructive remarks.

602

603 **References**

604

605 Amédro, F., 1992. L'Albien du bassin anglo-parisien: Ammonites zonation phylétique, sé-
606 quences. Bull. Centres Rech. Explor-Prod. Elf Aquitaine 16, 187-233.

607 Amédro, F., 2009. Stratigraphie séquentielle des successions albiennes du bassin anglo-pari-
608 sien et du bassin de Mons (Belgique). Bulletin d'Information des Géologues du Bassin
609 de Paris 46 (2) : 12-36.

610 Amédro, F., Matrimon, B., 2007. Une coupe lithologique synthétique dans l'Albien-type de
611 l'Aube. Bull. inf. géol. Bass. Paris 44, 7-23.

612 Amédro, F., Deconinck J.F., Matrimon, B., 2019. L'Albien type de l'Aube (France) : première
613 description litho-biostratigraphique de la totalité des Argiles tégulines de Courcelles.
614 Bull. inf. géol. Bass. Paris. In press.

615 Amédro, F., Matrimon, B., 2008. Corrélations dans l'Albien de l'Yonne et de l'Aube, France
616 (lithologie et ammonites). Bull. inf. géol. Bass. Paris 45, 12-24.

617 Amédro, F., Matrimon, B., 2014. L'étage Albien dans sa région-type, (Aube, France) : une
618 synthèse dans un contexte sédimentaire global. Carnets de Géologie 14, 5, 69-128.

619 Amédro, F., Matrimon, B., Deconinck J.-F., Huret, E. Landrein, P., 2017. Les forages de
620 Juzanvigny (Aube, France) : litho-biostratigraphie des formations du Barrémien à
621 l'Albien moyen dans l'est du bassin de Paris et datations par les ammonites.
622 Geodiversitas 39, 2, 185-212.

623 Amédro, F., Matrimon, B., Touch, R., 2000. La zone d'ammonite à *Protohoplites*
624 (*Hemisonneratia*) *puzosianus* et sa position dans la zonation réactualisée de l'Albien
625 inférieur du bassin anglo-parisien. Bull. inf. géol. Bass. Paris 37, 3-12.

626 Amédro F., Robaszynski F., 2014. Le Crétacé du Bassin parisien. In, Le Bassin parisien, un
627 nouveau regard sur la géologie. J.P.Gely & F. Hanot ed. Association des géologues du
628 Bassin de Paris, p. 75-84.

629 Banfield, J. F., Murakami, T., 1998. Atomic-resolution transmission electron microscope
630 evidence for the mechanism by which chlorite weathers to 1:1 semi-regular chlorite-
631 vermiculite. American Mineralogist, 83, 3-4, 348-357.

632 Barbarand, J., Bour, I., Pagel, M., Quesnel, F., Delcambre, B., Dupuis, C. & Yans, J., 2018.
633 Post-Paleozoic evolution of the northern Ardenne Massif constrained by apatite
634 fission-track thermochronology and geological data. BSGF - Earth Sciences Bulletin
635 189, 16. doi:10.1051/bsgf/2018015.

636 Blaise, T., Barbarand, J., Kars, M., Ploquin, F., Aubourg, C., Brigaud, B., Cathelineau, M., El
637 Albani, A., Gautheron, C., Izart, A., Janots, D., Michels, R., Pagel, M., Pozzi, J.P.,

638 Boiron, M.C. and Landrein, P., 2014. Reconstruction of low temperature (<100° C)
639 burial in sedimentary basins: A comparison of geothermometer in the intracontinental
640 Paris Basin. *Marine and Petroleum Geology* 53, 71-87.

641 Bodin, S., Meissner, P., Janssen, N.M.M., Steuber, T., Mutterlose J., 2015. Large igneous
642 provinces and organic carbon burial: Controls on global temperature and continental
643 weathering during the Early Cretaceous. *Global and Planetary Change* 133, 238–253.

644 Bomou, B., Deconinck, J.-F., Pucéat, E., Amédéo, F., Joachimski, M. M. Quillévéré, F., 2016.
645 Isotopic seawater temperatures in the Albian Gault Clay of the Boulonnais (Paris
646 Basin): palaeoenvironmental implications. *Proceedings of the Geologists' Association*
647 127, 699-711.

648 Boucot, A., J., Chen, X., Scotese, C., R., 2013. Phanerozoic paleoclimate: An atlas of
649 lithologic indicators of climate. Tulsa, USA: Society for Sedimentary Geology
650 (SEPM).

651 Bougeault, C., Pellenard, P., Deconinck, J.F., Hesselbo, S.P., Dommergues, J.L., Bruneau, L.,
652 Cocquerez, T., Laffont, R., Huret, E., Thibault, N., 2017. Climatic and
653 palaeoceanographic changes during the Pliensbachian (Early Jurassic) inferred from
654 clay mineralogy and stable isotope (C-O) geochemistry (NW Europe). *Global and*
655 *Planetary Change*, 149, 139-152.

656 Bréhéret, J.G., 1985a. Indices d'un événement anoxique étendu à la Téthys alpine, à l'Albien
657 inférieur (événement Paquier). *C.R. Acad. Sci., Paris* 300, II, 8, 355-358.

658 Bréhéret, J.G., 1985b. Sédimentologie et diagenèse de la matière organique contenue dans le
659 niveau Paquier, couche repère de l'Albien inférieur vocontien. *C.R. Acad. Sci., Paris*
660 301, II, 15, 1151-1156.

661 Bréhéret, J.G., 1997. L'Aptien et l'Albien de la Fosse vocontienne (des bordures au bassin).
662 Évolution de la sédimentation et enseignements sur les événements anoxiques. *Société*
663 *géologique du Nord*, Publ. n° 25, 644 p.

664 Brigaud, B., Vincent, B., Pagel, M., Gras, A., Noret, A., Landrein, P., Huret, E., 2018.
665 Sedimentary architecture, depositional facies and diagenetic response to intracratonic
666 deformation and climate change inferred from outcrops for a pivotal period
667 (Jurassic/Cretaceous boundary, Paris Basin, France). *Sedimentary Geology* 373, 48-
668 76.

669 Chaboureau, A.C., Sépulchre, P., Donnadiou, Y., Franc, A., 2014. Tectonic-driven climate
670 change and the diversification of angiosperms. *PNAS*. 111, 39, 14066–14070.

671 Chamley, H., 1989. *Clay Sedimentology*. Springer Verlag, Berlin, Heidelberg, 623 p.

672 Chumakov, N.M., Zharkov, M.A., Herman, A.B., Doludenko, M.P., Kalandadze, N.N.,
673 Lebedev, E.A., Ponomarenko, A.G., Rautian, A.S., 1995. Climate belts of the mid-
674 Cretaceous time. *Stratigr. Geol. Correl.* 3, 241–260.

675 Clauer, N., O’Neil, J.R., Bonnot-Courtois, C. and Holtzapffel, T., 1990. Morphological,
676 chemical, and isotopic evidence for an early diagenetic evolution of detrital smectite in
677 marine sediments. *Clays and Clay Minerals* 38, 1, 33-46.

678 Coiffard, C., Gomez, B., Thévenard, F., 2007. Early Cretaceous Angiosperm Invasion of
679 Western Europe and Major Environmental Changes. *Annals of Botany* 100, 545-553.

680 Damotte R., Magniez-Jannin F., 1973. Ostracodes et Foraminifères de l’Aptien inférieur du
681 sondage du Bois du Perchois (Aube). *Bull. Inf. Géol. Bass. Paris*, 36, 3-47.

682 Deconinck, J.F., Beaudoin, B., Chamley, H., Joseph, P. Raoult, J.F., 1985. Contrôles
683 tectonique, eustatique et climatique de la sédimentation argileuse du domaine subalpin
684 français au Malm-Crétacé. *Rev. Géol. Dyn. Géogr. Phys.* 26, 5, 311-320.

685 Deconinck, J.F., Chamley, H., 1983. Héritage et diagenèse des minéraux argileux dans les
686 alternances marno-calcaires du Crétacé inférieur du domaine subalpin. *C. R. Acad.*
687 *Sc.*, Paris 297, 589-594.

688 Deconinck, J.F., Chamley, H., 1995. Diversity of smectite origins in Late Cretaceous
689 sediments: example of chalks from northern France. *Clay minerals* 30, 365-379.

690 Deconinck, J.F. and Debrabant, P., 1985. Diagenèse des argiles dans le domaine subalpin:
691 rôle respectif de la lithologie, de l’enfouissement et de la surcharge tectonique. *Rev.*
692 *Géol. Dyn. Géogr. Phys.* 26, 5, 321-330.

693 Deconinck, J.F., Vanderaveroet, P., 1996. Eocene to Pleistocene clay mineral sedimentation
694 off New Jersey, western North Atlantic (sites 903 and 905). *Proceedings ODP Vol.*
695 *150 Scientific results*, 147 - 170.

696 Dellisanti, F., Pini, G.A., Baudin, F., 2010. Use of T_{max} as a thermal maturity indicator in
697 orogenic successions and comparison with clay mineral evolution. *Clay minerals* 45,
698 115-130.

699 Dera, G., Pellenard, P., Neige, P., Deconinck, J.-F., Pucéat, E. Dommergues, J.-L., 2009.
700 Distribution of clay minerals in Early Jurassic Peritethyan seas: Palaeoclimatic
701 significance inferred from multiproxy comparisons. *Palaeogeography,*
702 *Palaeoclimatology, Palaeoecology* 271, 39-51.

703 Erbacher, J., Hemleben, C., Huber, B.T., Markey, M., 1999. Correlating environmental
704 changes during early Albian oceanic anoxic event 1B using benthic foraminiferal
705 paleoecology. *Marine Micropaleontology* 38, 7-28.

706 Fauconnier, D., 1975. Répartition des Péridiniens de l'Albien du bassin de Paris. Rôle
707 stratigraphique et liaison avec le cadre sédimentologique. Bull. BRGM 4, 235-273.

708 Fenner, J., 2001. Middle and Late Albian geography, oceanography, and climate and the
709 setting of the Kirchrode I and II borehole sites. Palaeogeography, Palaeoclimatology,
710 Palaeoecology 174, 5-32.

711 Ferry, S., Cotillon, P. and Rio, M., 1983. Diagenèse croissante des argiles dans les niveaux
712 isochrones de l'alternance calcaire-marne valanginienne du bassin vocontien. Zonation
713 géographique. C.R. Acad. Sci. Paris 297, 51-56.

714 Fielitz, W, Mansy, J-L., 1999. Pre- and synorogenic burial metamorphism in the Ardenne and
715 neighbouring areas (Renohercynian zone, central European Variscides). In: Sintubin
716 M, Vandycke S, Camelbeeck T, eds. Palaeozoic to recent tectonics in the NW
717 European Variscan front zone. Tectonophysics 309, 227–256.

718 Föllmi, K.B., 2012. Early Cretaceous life, climate and anoxia. Cretaceous Research, 35, 230-
719 257.

720 Friedrich, O., Norris, R.D., Erbacher, J., 2012. Evolution of middle to Late Cretaceous
721 oceans—A 55 m.y. record of Earth's temperature and carbon cycle. Geology 40, 2,
722 107-110.

723 Friès, G., 1987. Dynamique du bassin subalpin méridional de l'Aptien au Cénomanién. École
724 des Mines de Paris. Mémoire des sciences de la Terre 4, 370 p.

725 Gale, A.S., Huggett, J.M. Gill, M., 1996. The stratigraphy and petrography of the Gault Clay
726 Formation (Albian, Cretaceous) at Redcliff, Isle of Wight. Proceedings of the
727 Geologists' Association 107, 287-298.

728 Gale, A.S., Bown, P., Caron, M., Crampton, J., Crowhurst, S.J., Kennedy, W.J., Petrizzo,
729 M.R. Wray, D.S., 2011. The uppermost Middle and Upper Albian succession at the
730 Col de Palluel, Hautes-Alpes, France: an integrated study (ammonites, inoceramid
731 bivalves, planktonic foraminifera, nannofossils, geochemistry, stable oxygen and
732 carbon isotopes, cyclo- stratigraphy). Cretaceous Research 32, 59-130.

733 Gély, J.-P. Hanot F., (dir.). 2014. Le bassin parisien, un nouveau regard sur la géologie.
734 Bulletin d'Information des Géologues du Bassin de Paris, Mémoire hors-série 9, 228
735 p., 1 pl.

736 Ghirardi, J., Deconinck, J.F., Pellenard, P., Martinez, M., Bruneau, L., Amiotte-Suchet, P.
737 Pucéat, E., 2014. Multi-proxy orbital chronology in the aftermath of the Aptian
738 Oceanic Anoxic Event 1a : Palaeoceanographic implications (Serre Chaitieu section,
739 Vocontian Basin, SE France). Newsletters on Stratigraphy 47, 3, 247-262.

740 Gibbs, R.J., 1977. Clay mineral segregation in the marine environment. *J. Sedimentary*
741 *Research*, 47, 237–243.

742 Godet, A., Bodin, S., Adatte, T. and Föllmi, K.B., 2008. Platform-induced clay-mineral
743 fractionation along a northern Tethyan basin-platform transect: implications for the
744 interpretation of Early Cretaceous climate change (Late Hauterivian-Early Aptian).
745 *Cretaceous Research* 29, 830–847.

746 Guillocheau, F., Robin, C., Allemand, P., Bourquin, S., Brault, N., Dromart, G., Friedenber,
747 R., Garcia, J.-P., Gaulier, J.-M., Gaumet, F., Grosdoy, B., Hanot, F., Le Strat, P.,
748 Mettraux, M., Nalpas, T., Prijac, C., Rigollet, C., Serrano, O. Grandjean, G., 2000.
749 Meso-Cenozoic geodynamic evolution of the Paris Basin: 3D stratigraphic constraints.
750 *Geodinamica Acta* 13, 189–246.

751 Han, G., Pr at, A., Chamley, H., Deconinck, J.F., Mansy, J.L., 2000. Palaeozoic clay mineral
752 sedimentation and diagenesis in the Dinant and Avesnes basins (Belgium, France):
753 relationships with variscan tectonism. *Sedimentary Geology* 136, 3-4, 217-238.

754 Haq B.U., 2014. Cretaceous eustasy revisited. *Global and Planetary Change*, 113, 44-58

755 Hardenbol, J., Thierry, J., Farley, M. B., Jacquin, T., de Graciansky, P.-C. Vail, P. R., 1998.
756 Mesozoic and Cenozoic Sequence chronostratigraphic framework of European Basins,
757 *in de Graciansky P.-C., Hardenbol J., Jacquin T. and Vail P. R. (Eds.), Mesozoic-*
758 *Cenozoic Sequence Stratigraphy of European Basins. SEPM Special Publication* 60, 3-
759 13.

760 Hart, M., Am dro, F. Owen, H., 1996. The Albian stage and substage boundaries. *Bulletin de*
761 *l’institut royal des sciences naturelles de Belgique*, vol. 66 (suppl.), *Comptes-rendus* «
762 *Second International Symposium on Cretaceous Stage Boundaries* », Bruxelles 8-16
763 septembre 1995, 45-56.

764 Hay, W.W., Floegel, S., 2012. New thoughts about the Cretaceous climate and oceans. *Earth*
765 *Science Reviews* 115, 262-272.

766 Heimhofer, U., Hochuli, P.A., Burla, S., Oberli, F., Adatte, T., Dinis, J.L., Weissert, H., 2012.
767 Climate and vegetation history of western Portugal inferred from Albian near-shore
768 deposits (Gal  Formation, Lusitanian Basin). *Geological Magazine* 149, 1046-1064.

769 Heimhofer, U., Adatte, T., Hochuli, P.A., Burla, S., Weissert, H., 2008. Coastal sediments
770 from the Algarve: low-latitude climate archive for the Aptian-Albian. *Int. J. Earth Sci.*
771 *(Geol Rundsch)* 97, 785–797.

772 Herbillon, A.J. Makumbi, M.N., 1975. Weathering of chlorite in a soil derived from a
773 chloritoschist under humid tropical conditions. *Geoderma* 13, 89-104.

774 Herrle, J.O., Mutterlose, J., 2003. Calcareous nannofossils from the Aptian–Lower Albian of
775 southeast France: palaeoecological and biostratigraphic implications. *Cretaceous*
776 *Research* 24, 1-22.

777 Herrle, J.O., Pross, J., Friedrich, O., Hemleben, C., 2003a. Short-term environmental changes
778 in the Cretaceous Tethyan Ocean: micropalaeontological evidence from the Early
779 Albian Oceanic Anoxic Event 1b. *Terra Nova* 15, 14-19.

780 Herrle, J.O., Pross, J., Friedrich, O., Köbber, P., Hemleben, C., 2003b. Forcing mechanisms
781 for mid-Cretaceous black shale formation: evidence from Upper Aptian and Lower
782 Albian of the Vocontian Basin (SE France). *Palaeogeography, Palaeoclimatology,*
783 *Palaeoecology* 190, 399-426.

784 Hofmann, P., Stüsser, I., Wagner, T., Schouten, S., Sinninghe Damsté, J.S., 2008. Climate–
785 ocean coupling off North-West Africa during the Lower Albian: The Oceanic Anoxic
786 Event 1b. *Palaeogeography, Palaeoclimatology, Palaeoecology* 262, 157–165.

787 Holtzapffel, T., 1985. Smectites authigènes et glauconitisation dans les Argiles du Gault
788 (Albien du Boulonnais). *Ann. Soc. Géol. Nord, Lille, CIV*, 33-39.

789 Holtzapffel, T., 1987. Assemblages argileux de nodules phosphatés et de leur matrice dans les
790 argiles albiennes du Boulonnais (France). *Ann. Soc. Géol. Nord, Lille, CVI*, 267-273.

791 Holtzapffel, T., Bonnot-Courtois, C., Chamley, H., Clauer, N., 1985. Respective influence of
792 detrital supply and marine diagenesis on the formation of Albo-Aptian and Paleogene
793 smectites in the North-Atlantic Range. *Bull. Soc. Géol. Fr.* 1, 25-33.

794 Horikx, M., Huck, S., Adatte, T., and Heimhofer, U., 2017. Vegetation dynamics, angiosperm
795 radiation and climatic changes in the Lusitanian Basin (Portugal) during Albian times.
796 *Palaeogeography, Palaeoclimatology, Palaeoecology* 465, 30-41.

797 Huber, B.T., MacLeod, K.G., Watkins, D.K., Coffin, M.F., 2018. The rise and fall of the
798 Cretaceous Hot Greenhouse climate. *Global and Planetary Change* 167, 1-23.

799 Jeans, C.V., Mitchell, J.G., Fisher, M.J., Wray, D.S. Hall, I.R. 2001. Age, origin and climatic
800 signal of English Mesozoic clays based on K/Ar signatures. *Clay minerals* 36, 515-
801 539.

802 Jenkyns, H.C., 2010. Geochemistry of oceanic anoxic events. *Geochemistry, Geophysics,*
803 *Geosystems*, 11, 3.

804 Kanungo, S., Bown, P.R., Young, J.R. and Gale, A.S., 2018. A brief warming event in the late
805 Albian: evidence from calcareous nannofossils, macrofossils, and isotope
806 geochemistry of the Gault Clay Formation, Folkestone, southeastern England. *J.*
807 *Micropalaeontology* 37, 231–247.

808 Kennedy, W.J., Gale, A.S., Bown, P.R., Caron, M., Davey, R.J., Gröcke, D., Wray, D.J.,
809 2000. Integrated stratigraphy across the Aptian-Albian boundary in the Marnes Bleues,
810 at the Col de Pré-Guittard, Arnayon (Drôme), and at Tartonne (Alpes-de-Haute-
811 Provence), France, a candidate Global Boundary Stratotype Section and Point for the
812 base of the Albian Stage. *Cretaceous Research* 21, 591-720.

813 Kennedy, W.J., Gale, A.S., Huber, B.T., Petrizzo, M.R., Bown, P., Barchetta, A., Jenkyns,
814 H.C., 2014. Integrated stratigraphy across the Aptian/Albian boundary at Col de Pré-
815 Guittard (southeast France): A candidate Global Boundary Stratotype Section.
816 *Cretaceous Research* 51, 248-259.

817 Kennedy, W.J., Gale, A.S., Huber, B.T., Petrizzo, M.R., Bown, P., Barchetta, A. and Jenkyns,
818 H.C., 2017. The Global Boundary Stratotype Section and Point (GSSP) for the base of
819 the Albian Stage, of the Cretaceous, the Col de Pré-Guittard section, Arnayon, Drôme,
820 France. *Journal of International Geoscience* 40, 177-188.

821 Knight, R. I., 1999. Phosphates and phosphogenesis in the Gault Clay (Albian) of the Anglo-
822 Paris Basin. *Cretaceous Research* 20, 507-521.

823 Kühn, V., Heydemann, A., Usdowski, E., 2001. Mineralogy of the upper Albian sediments
824 from the Kirchrode I borehole with special emphasis on the clay mineralogy. *Palaeo-
825 geography, Palaeoclimatology, Palaeoecology* 174, 145-159.

826 Lanson, B., Sakharov, B. A., Claret, F. Drets, V.A., 2009. Diagenetic smectite-to-illite
827 transition in clay-rich sediments: a reappraisal of X-ray diffraction results using the
828 multi-specimen method. *Am. J. Science* 309, 476-516.

829 Levert, J. Ferry, S., 1988. Diagenèse argileuse complexe dans le mésozoïque subalpin révélée
830 par cartographie des proportions relatives d'argiles selon des niveaux isochrones. *Bull.
831 Soc. Géol. Fr.* 4, 1029-1038.

832 Li, P., Zhang, C., Guo Z., Deng, C., Ji, X., Jablonski, N.G., Wu, H., Zhu, R. 2019. Clay
833 mineral assemblages in the Zhaotong Basin of southwestern China: Implications for
834 the late Miocene and Pliocene evolution of the South Asian monsoon. *Palaeogeography,
835 Palaeoclimatology, Palaeoecology*, 516, 90-100.

836 Mangenot, X., Gasparrini, M., Rouchon, V., Bonifacie, M., 2018. Basin-scale thermal and
837 fluid flow histories revealed by carbonate clumped isotopes (Δ_{47}) – Middle Jurassic
838 carbonates of the Paris Basin depocentre. *Sedimentology*, 65, 123-150.

839 Martinez, M., Deconinck, J.F., Pellenard, P., Reboulet, S., Riquier, L., 2013. Astrochronology
840 of the Valanginian Stage from reference sections (Vocontian Basin, France) and

841 palaeoenvironmental implications for the Weissert Event. *Palaeogeography,*
842 *Palaeoclimatology, Palaeoecology* 376, 91-102.

843 Merriman, R.J. Frey, M., 1999. Patterns of very low-grade metamorphism in metapelitic
844 rocks. In: Frey, M., Robinson, D. (Eds.). *Low-Grade Metamorphism*. Blackwell
845 Science Ltd, 61-107.

846 Meyer, K.W. Petersen, S.V., Lohmann, K.C., Winkelstern, I.Z., 2018. Climate of the Late
847 Cretaceous North American Gulf and Atlantic Coasts. *Cretaceous research* 89, 160-
848 173.

849 Millán, M. I., H. J. Weissert, and M. A. López-Horgue, 2014, Expression of the late Aptian
850 cold snaps and the OAE1b in a highly subsiding carbonate platform (Aralar, northern
851 Spain): *Palaeogeography Palaeoclimatology Palaeoecology*, v. 411, p. 167-179.

852 Moore, D.M., Reynolds, R.C., 1997. X-Ray diffraction and the identification and Analysis of
853 Clay Minerals; second edition (23) ; Oxford, New York : Oxford University Press :
854 378 p.

855 Mutterlose J., Bornemann A., Luppold F.W., Owen H.G., Ruffell A., Weiss W., & Wray D.
856 2003. The Vöhrum section (northwest Germany) and the Aptian/Albian boundary.
857 *Cretaceous Research.*, 23, 203-252.

858 Myers, K.J., Wignall, P.B., 1987. Understanding Jurassic organic-rich mudrocks — new
859 concepts using gamma-ray spectrometry and palaeoecology: examples from the
860 Kimmeridge Clay of Dorset and the Jet Rock of Yorkshire. In: Legget, J.K., Zuffa,
861 G.G. (Eds.), *Marine Clastic Environments: Concepts and Case Studies*. Graham and
862 Trotman, London, 172–189.

863 O'Brien, C.L., Robinson, S.A., Pancost, R.D et al., 2017. Cretaceous sea-surface temperature
864 evolution: Constraints from TEX86 and planktonic foraminiferal oxygen isotopes.
865 *Earth-Science Reviews* 172, 224-247.

866 Owen, H.G., 1971. The Stratigraphy of the Gault in the Thames Estuary and its Bearing on
867 the Mesozoic Tectonic History of the Area. *Proceedings of the Geologists'*
868 *Association* 82, 2, 187-208.

869 Owen, H.G., 1999. Correlation of Albian European and Tethyan ammonite zonation and the
870 boundaries of the Albian Stage and substages: some comments. *Scripta Geologica,*
871 *Special Issue* 3, 129-149.

872 Pellenard, P., Deconinck, J.F., Marchand, D., Thierry, J., Fortwengler, D., Vigneron G., 1999.
873 *Contrôle géodynamique de la sédimentation argileuse du Callovien-Oxfordien moyen*

874 dans l'Est du Bassin de Paris : influence eustatique et volcanique. C.R. Acad; Sci,
875 Paris 328, 807-813.

876 Pictet, A., Mojon, P.O., Matrimon, B., Adatte, T., Spangenberg, J.E., Föllmi, K.B., 2019.
877 Record of latest Barremian-Cenomanian environmental change in tectonically
878 controlled depressions from the Jura-Burgundy threshold (Jura Mountains, eastern
879 France and western Switzerland). *Palaeogeography, Palaeoclimatology, Palaeoecology*
880 514, 627-654.

881 Pirrie, D., Marshall, J.D., Doyle, P. Riccardi, A.C., 2004. Cool early Albian climates; new
882 data from Argentina. *Cretaceous Research* 25, 27-33.

883 Petrizzo, M.R., Huber, B.T., Gale, A.S., Barchetta, A., Jenkyns, H.C., 2012. Abrupt planktic
884 foraminiferal turnover across the Niveau Kilian at Col de Pré-Guittard (Vocontian
885 Basin, southeast France): new criteria for defining the Aptian/Albian boundary.
886 *Newsletters on Stratigraphy* 45, 1, 55-74.

887 Pomerol, B., 1986. Minéralogie des argiles albiennes du sud du Pays d'Othe (sud-est du
888 bassin de Paris). Modalités du passage latéral Sables de la Puisaye-Argiles Tégulines.
889 *Géologie de la France* 1, 139-149.

890 Poulsen, C.J., Barron, R.J., Arthur, M.A., Peterson, W.H., 2001. Response of the mid-
891 Cretaceous global oceanic circulation to tectonic and CO₂ forcings. *Paleoceanography*
892 16, 6, 576-592.

893 Proust, D., Eymery, J.P. Beaufort, D., 1986. Supergene vermiculitization of a magnesian
894 chlorite: iron and magnesium removal processes. *Clays and Clay Minerals* 34, 5, 572-
895 580.

896 Quesnel, F., 2003. Paleoweathering and paleosurfaces from northern and eastern France to
897 Belgium and Luxembourg: geometry, dating and geodynamic implications. *Géologie*
898 *de la France* 1, 95-104.

899 Rat, P., Magniez-Jannin, F., Chateauneuf, J.-J., Damotte, R., Destombes, P., Fauconnier, D.,
900 Feuillée, P., Manivit, H., Mongin, D., Odin, G.S., 1979. L'Albien de l'Aube. *Les*
901 *stratotypes français*, Paris, 5, 446 p., 51 pl.

902 Righi, D., Petit, S., Bouchet, A., 1993. Characterization of Hydroxy-Interlayered Vermiculite
903 and Illite/Smectite Interstratified Minerals from the Weathering of Chlorite in a
904 Cryorthod. *Clays and Clay Minerals* 41, 4, 484-495.

905 Robaszynski, F., Pomerol, B., Masure, E., Bellier, J.P., Deconinck, J.F., 2005. Stratigraphy
906 and stage boundaries in a type-section of the Late Cretaceous chalk from the East Paris
907 basin: The "Craie 700 boreholes" *Cretaceous Research* 26, 2, 157-169.

908 Rodríguez-López, J.P., Liesa, C.L., Pardo, G., Meléndez, N., Soria, A.R. Skillinga, I., 2016.
909 Glacial dropstones in the western Tethys during the late Aptian–early Albian cold
910 snap: Palaeoclimate and palaeogeographic implications for the mid-Cretaceous.
911 *Palaeogeography, Palaeoclimatology, Palaeoecology* 452, 11–27.

912 Ruffell, A., 2016. Do spectral gamma ray data really reflect humid–arid palaeoclimates? A
913 test from Palaeogene Interbasaltic weathered horizons at the Giant’s Causeway, N.
914 Ireland. *Proceedings of the Geologists' Association* 127, 18-28.

915 Ruffell, A., McKinley, J.M. Worden, R.H., 2002. Comparison of clay mineral stratigraphy to
916 other proxy palaeoclimate indicators in the Mesozoic of NW Europe. *Philosophical*
917 *Transactions of the Royal Society London A* 360, 675-693.

918 Ruffell, A. Garden, R., 1997. Tectonic controls on the variation in thickness and mineralogy
919 of pebble-beds in the Lower Greensand Group (Aptian-Albian) of the Isle of Wight,
920 southern England. *Proceedings of the Geologists' Association* 108, 215-229.

921 Sabatino, N., Coccioni, R., Manta, D. S., Baudin, F., Vallefucio, M., Traina, A. Sprovieri,
922 M., 2015. High-resolution chemostratigraphy of the late Aptian-early Albian oceanic
923 anoxic event (OAE 1b) from the Poggio le Guaine section (Umbria-Marche Basin,
924 central Italy). *Palaeogeography, Palaeoclimatology, Palaeoecology* 426, 319-333.

925 Sender, L. M., Diez, J. B., Ferrer, J., Pons, D., Rubio, C., 2005. Preliminary data on a new
926 Albian flora from the Valle del Río Martín Teruel, Spain. *Cretaceous Research*, 26, 6,
927 898-905.

928 Środoń, J., Clauer, N., Huff, W., Dudek, T. Banaś, M., 2009. K-Ar dating of the Lower
929 Palaeozoic K-bentonites from the Baltic Basin and the Baltic Shield: implications for
930 the role of temperature and time in the illitization of smectite. *Clay minerals* 44, 361–
931 387.

932 Steinberg, M., Holtzapffel, T. Rautureau, M., 1987. Characterization of overgrowth structures
933 formed around individual clay particles during early diagenesis. *Clays and Clay*
934 *Minerals* 35, 3, 189-195.

935 Thiry, M., 2000. Palaeoclimatic interpretation of clay minerals in marine deposits : an outlook
936 from the continental origin. *Earth-Science Reviews* 49, 1-4, 201-221.

937 Thiry, M., Quesnel, F., Yans, J., Wyns, R., Vergari, A., Théveniaut, H., Simon-Coinçon, R.,
938 Ricordel, C., Moreau, M.G., Giot, D., Dupuis, C., Bruxelles, L., Barbarand, J. Baele,
939 J.M., 2006. Continental France and Belgium during the early Cretaceous:
940 paleoweatherings and paleolandforms. *Bull. Soc. Géol. Fr.* 177, 3, 155-175.

- 941 Thiry, M., Simon-Coinçon, R., Quesnel, F. Wyns, R., 2005. Altération bauxitique associée
942 aux argiles à chailles sur la bordure sud-est du bassin de Paris. Bull. Soc. Géol. Fr.
943 176, 2, 199-214.
- 944 Tribovillard, N.-P. Gorin, G.E., 1991. Organic facies of the Early Albian Niveau Paquier, a
945 key black shales horizon of the Marnes Bleues Formation in the Vocontian Trough
946 (Subalpine Ranges, SE France). Palaeogeography, Palaeoclimatology, Palaeoecology
947 85, 227-237.
- 948 Ufnar, D.F., González, L.A., Ludvigson, G.A., Brenner, R.L., Witzke, B.J., 2002. The mid-
949 Cretaceous water bearer: Isotope mass balance quantification of the Albian hydrologic
950 cycle. Palaeogeography, Palaeoclimatology, Palaeoecology 188, 51-71.
- 951 Ufnar, D.F., González, L.A., Ludvigson G.A., Brenner R.L. Witzke B.J., 2004. Evidence for
952 increased latent heat transport during the Cretaceous (Albian) greenhouse warming.
953 Geology 32, 12, 1049-1052.
- 954 Weaver, C.E., 1989. Clays, muds and shales. Elsevier, Dev. Sedimentology, 44, 818 p.
- 955 Yans, J., 2003. An overview of the saprolites of Belgium and their potential kaolinitic
956 supplies to Mesozoic and Cainozoic sediments. Géologie de la France 1, 33-37.
- 957 Young, J. R., Gale, A. S., Knight, R. I., and Smith, A. B. (Eds.): Palaeontological Association
958 Field Guide to Fossils, 12, 312 pp., Palaeontological Association, UK, 2010.

959
960

961 **FIGURE CAPTIONS**

962

963 Figure 1. Palaeogeographic map (Albian) showing the location of the studied areas and the
964 boundary between the semi-arid and the mid latitude warm-humid belts defined by
965 Chumakov et al. (1995). Abbreviations: AM = Armorican Massif, BT = Burgundy
966 threshold, MC = Massif Central, IbM = Iberian Massif, LBM = London-Brabant
967 Massif, CS = Corso-Sarde microcontinent (modified from Amédro and Matrimon,
968 2014).

969 Figure 2. Location of the boreholes studied to the south-east of the Paris Basin (Amédro et al.,
970 2019).

971 Figure 3. Lithology, biostratigraphy and clay mineralogy of the AUB 111 borehole.
972 Abbreviations: SVA = 'Sables Verts de l'Aube', APT = Aptian, (K+C)/S =
973 (kaolinite+chlorite)/smectite.

974 Figure 4. Lithology, biostratigraphy and clay mineralogy of the AUB220 borehole. The
975 detailed lithological description and the biostratigraphic data were published by
976 Amédro et al. (2017). Abbreviations : SVA = ‘Sables Verts de l’Aube’, APT = Aptian,
977 (K+C)/S = (kaolinite+chlorite)/smectite.

978 Figure 5. Correlation between AUB111, AUB220 and AUB240 boreholes

979 Figure 6. Phosphatic crust corresponding to a hardground at the transition between the ‘Sables
980 Verts de l’Aube’ (Greensands) and the Argiles tégulines de Courcelles Formation in
981 borehole AUB220 (74.50 m in depth).

982 Figure 7. Lithology, biostratigraphy and clay mineralogy of the AUB 240 borehole. The
983 detailed lithological description is given in Amédro et al. (2019). (K+C)/S =
984 (kaolinite+chlorite)/smectite.

985 Figure 8. Detailed geographical location of the Col de Pré-Guittard section and field views of
986 this section.

987 Figure 9. Diffractograms obtained for the sample AUB220 – 25,50 m. The minerals identified
988 are : S = smectite (I/S R0), V = vermiculitic clays, C =chlorite, I = illite, K = kaolinite,
989 C/V = interstratified chlorite – vermiculite, Qtz = quartz.

990

991 Figure 10. Lithology, clay mineralogy and spectral gamma ray of the Col de Pré-Guittard
992 section. (K+C)/S = (kaolinite+chlorite)/smectite.

993 Figure 11. A. Palaeogeographic map, facies (modified after Amédro and Matrimon, 2014) and
994 inferred detrital clay mineral sources in the Paris and Vocontian basins. IW = Isle of
995 Wight, LBM = London-Brabant Massif.

996 B. Correlation between the AUB 220 borehole (Paris Basin) and the Col de Pré-
997 Guittard section (Vocontian Basin).

998 Table 1. Correspondences between the ammonite biozonations from the Paris and
999 Vocontian basins. The appearance of the foraminifer *Microhedbergella renilaevis* is
1000 marked in the *H. jacobi* zone. Abbreviations: U. Apt. = upper Aptian, *H. jacobi* =
1001 *Hypacanthoplites jacobi*, *Micr. renil.* = *Microhedbergella renilaevis*, *L. schrammeni* =
1002 *Proleymeriella schrammeni*, *L. germanica* = *Leymeriella germanica*, *L. tardefurcata*
1003 = *Leymeriella tardefurcata*, *L. regularis* = *Leymeriella regularis*, *S. kitchini* =
1004 *Sonneratia kitchini*, *C. floridum* = *Cleoniceras floridum*, *H. puzosiana* =
1005 *Hemisonneratia puzosiana*, *O. subhilli* = *Otohoplites subhilli*, *H. steinmanni* =
1006 *Hoplites (Isohoplites) steinmanni*, *D. mammillatum* = *Douvilleiceras mammillatum*,
1007 *L.l.* = *Lyelliceras lyelli*, *L. ps.* = *Lyelliceras pseudolyelli*, *H. benettianus* = *Hoplites*

1008 (*Hoplites*) *benettianus*, *H. dentatus* = *Hoplites dentatus*, *A. intermedius* = *Anahoplites*
1009 *intermedius*, *D. niobe* = *Dimorphoplites niobe*, *D. biplicatus* = *Dimorphoplites*
1010 *biplicatus*, *O. roissyanum* = *Oxytropidoceras roissyanum*, *D. cristatum* = *Dipoloceras*
1011 *cristatum*, *M. pricei* = *Mortoniceras pricei*, *M. inflatum* = *Mortoniceras inflatum*.

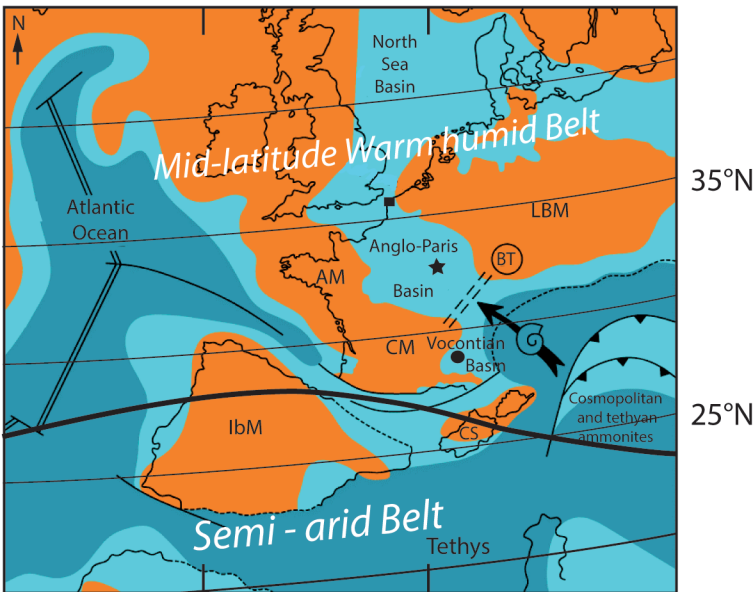
1012

1013

1014

30°W

20°W


 Oceans


 Epicontinental seas

 Emerged areas

 Wissant section

 "Col de Pré-Guittard" section

 Cores from the Aube department

 Boundary between the semi-arid and the humid belts

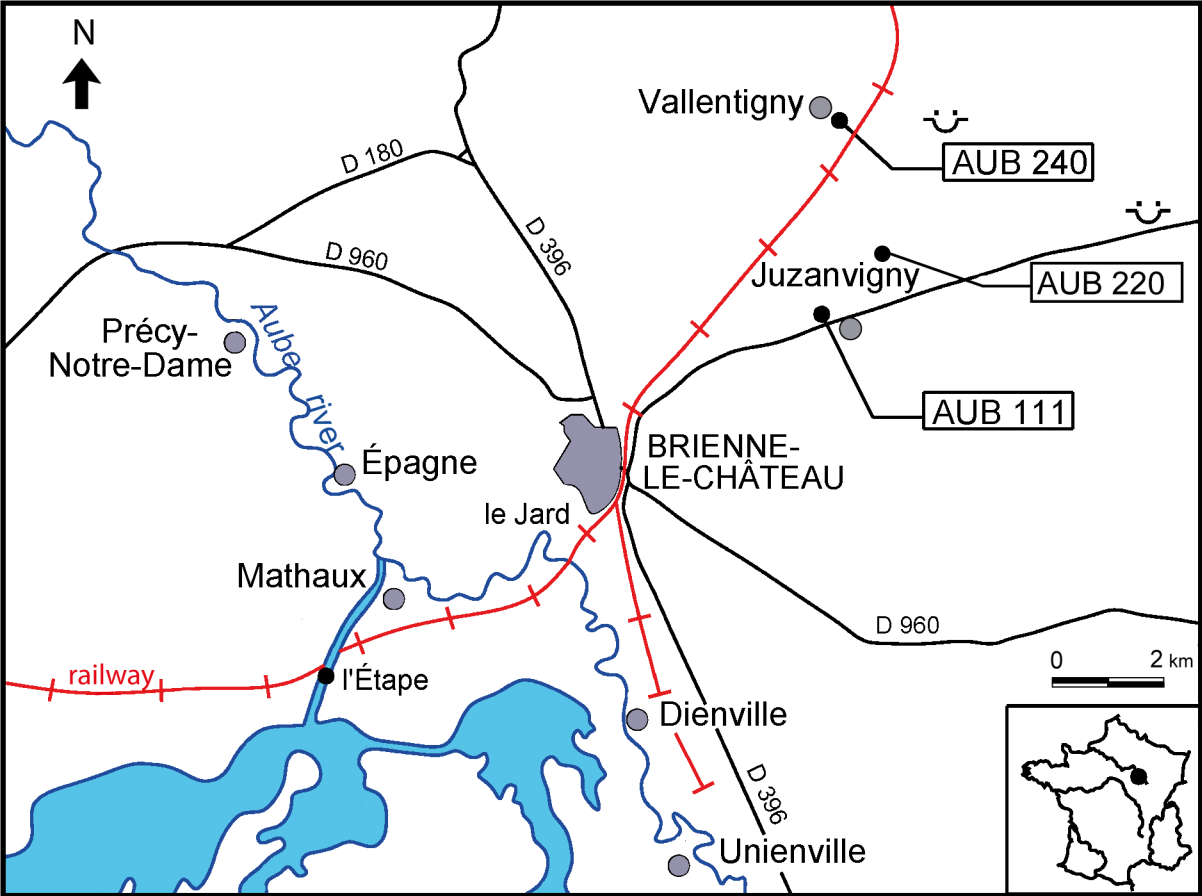
 High area

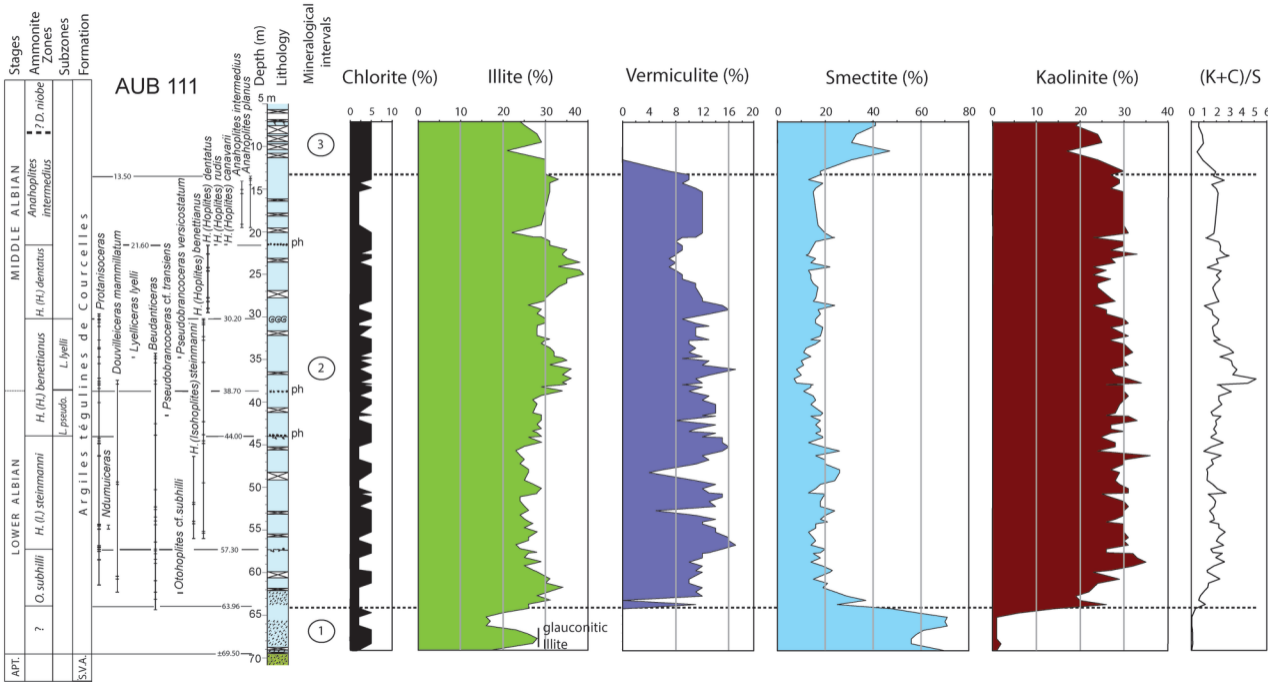
 Collision zone

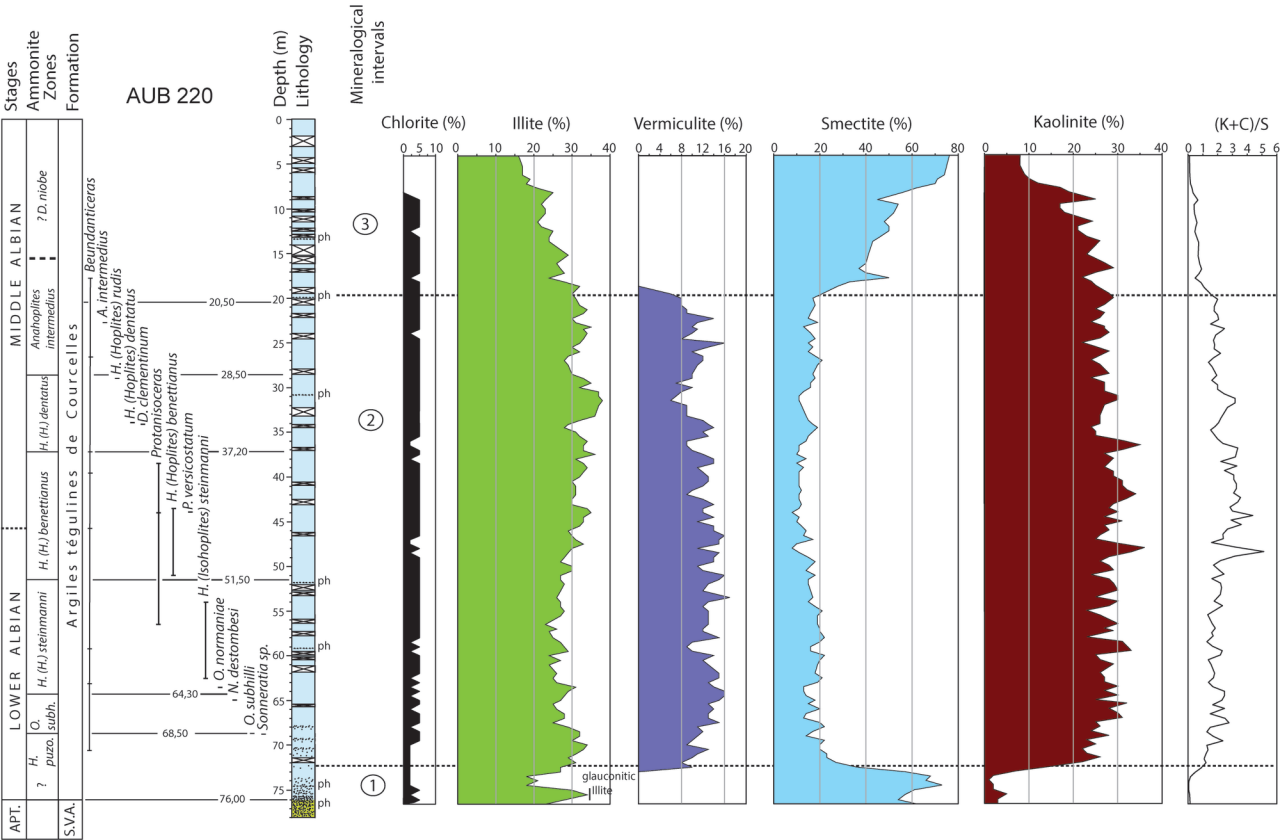
 Faults

 Oceanic Ridge

 Faunal arrivals

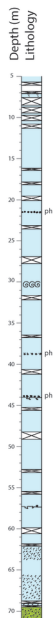




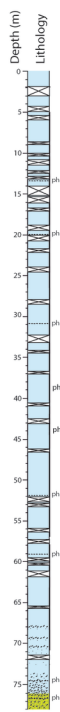


Stage
Zone
Formations

APT.			MIDDLE ALBIAN	
			<i>H. (H.) dentatus</i>	<i>Anahapilites intermedius</i> + <i>D. noble</i>
			<i>H. (H.) benettianus</i>	
			<i>H. (H.) steinmanni</i>	
			<i>O. subtilis</i>	
			?	
S.V.A.			Argiles tégulines de Courcelles	



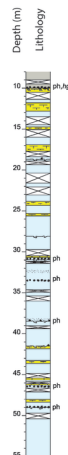
APT.			MIDDLE ALBIAN	
			<i>H. (H.) dentatus</i>	<i>Anahapilites intermedius</i> + <i>D. noble</i>
			<i>H. (H.) benettianus</i>	
			<i>H. (H.) steinmanni</i>	
			<i>H. puzosiana</i>	
			<i>O. subtilis</i>	
S.V.A.			Argiles tégulines de Courcelles	



Legend

- Kaolinite
- Smectite (%)
- Illite (%)
- Vermiculite (%)

			MIDDLE ALBIAN	
			<i>H. (H.) dentatus</i>	<i>Discopapilites</i> + <i>Discopapilites</i>
			<i>Anahapilites</i> + <i>Discopapilites</i>	<i>Anahapilites</i> + <i>Discopapilites</i>
			<i>H. (H.) benettianus</i>	
			<i>H. (H.) steinmanni</i>	
			<i>H. puzosiana</i>	
			<i>O. subtilis</i>	
			Argiles tégulines de Courcelles	
			UPPER ALBIAN	
			<i>Monsieurville (Monsieurville) infimus</i>	
			<i>Monsieurville (Monsieurville) proter</i>	
			Membre de Bièvre	



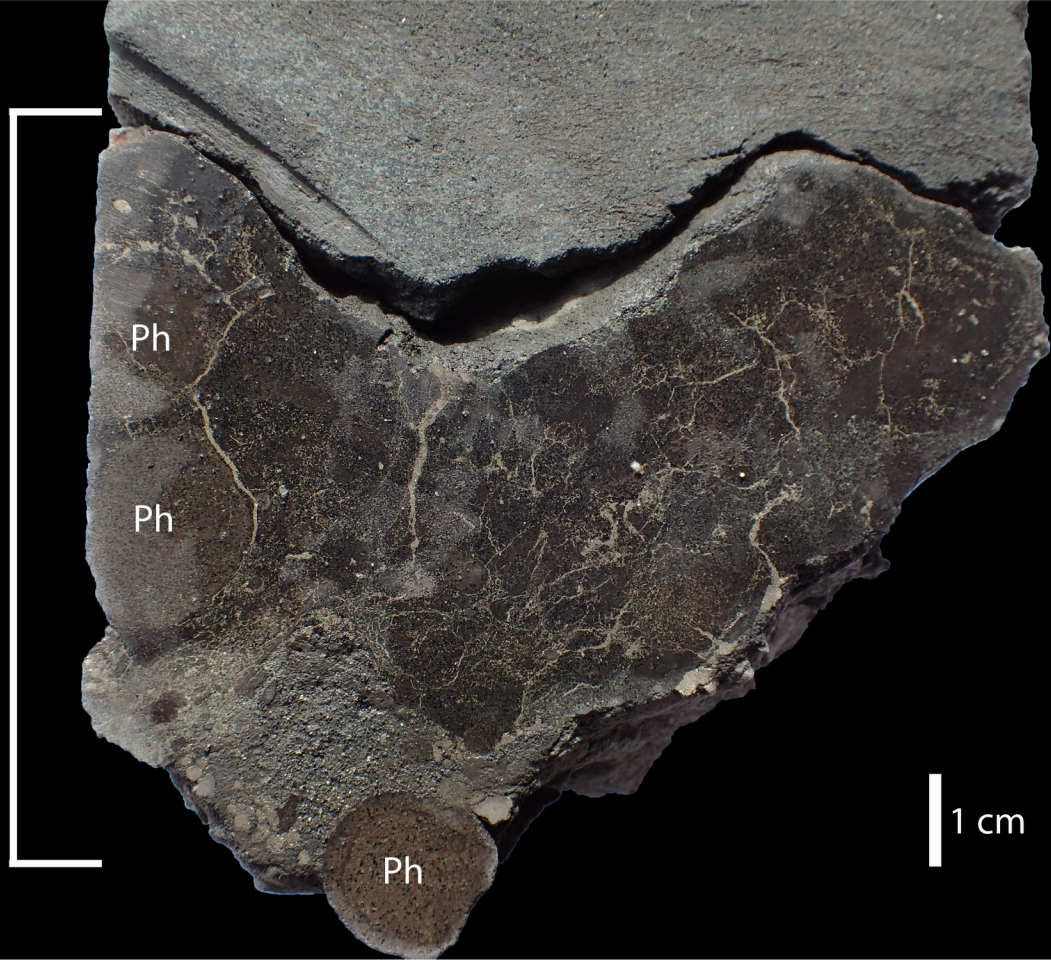
Hardground

Ph

Ph

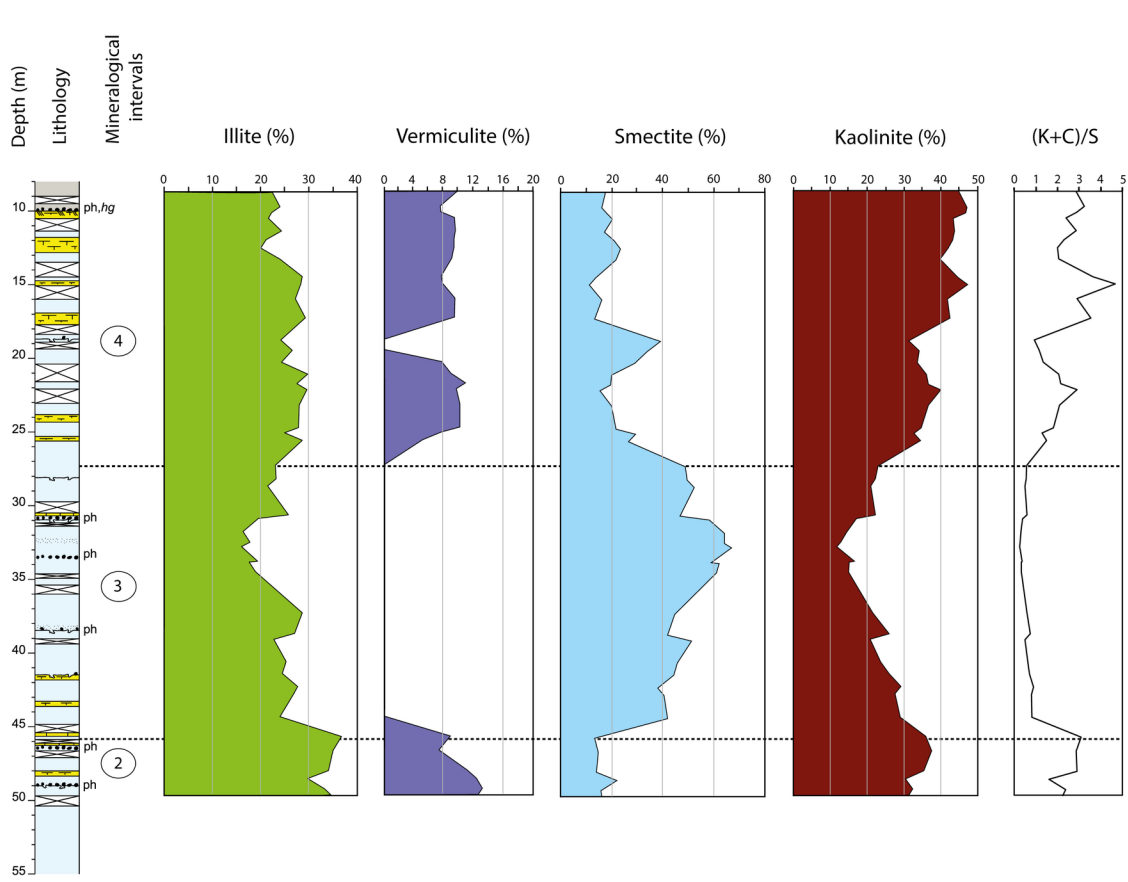
Ph

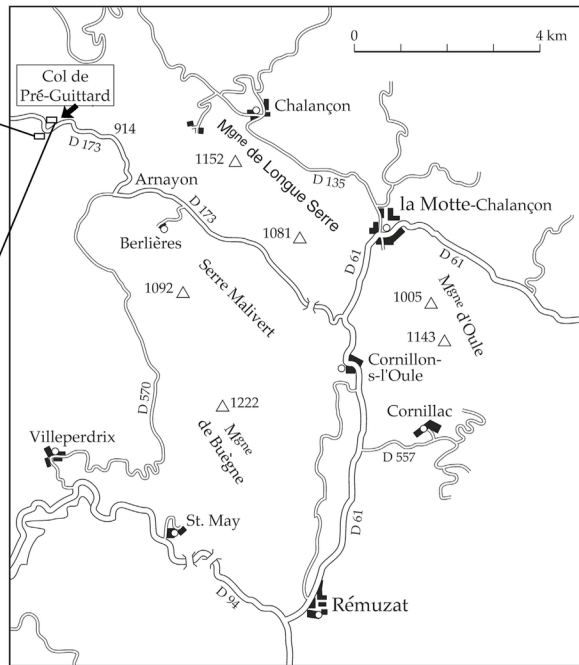
1 cm

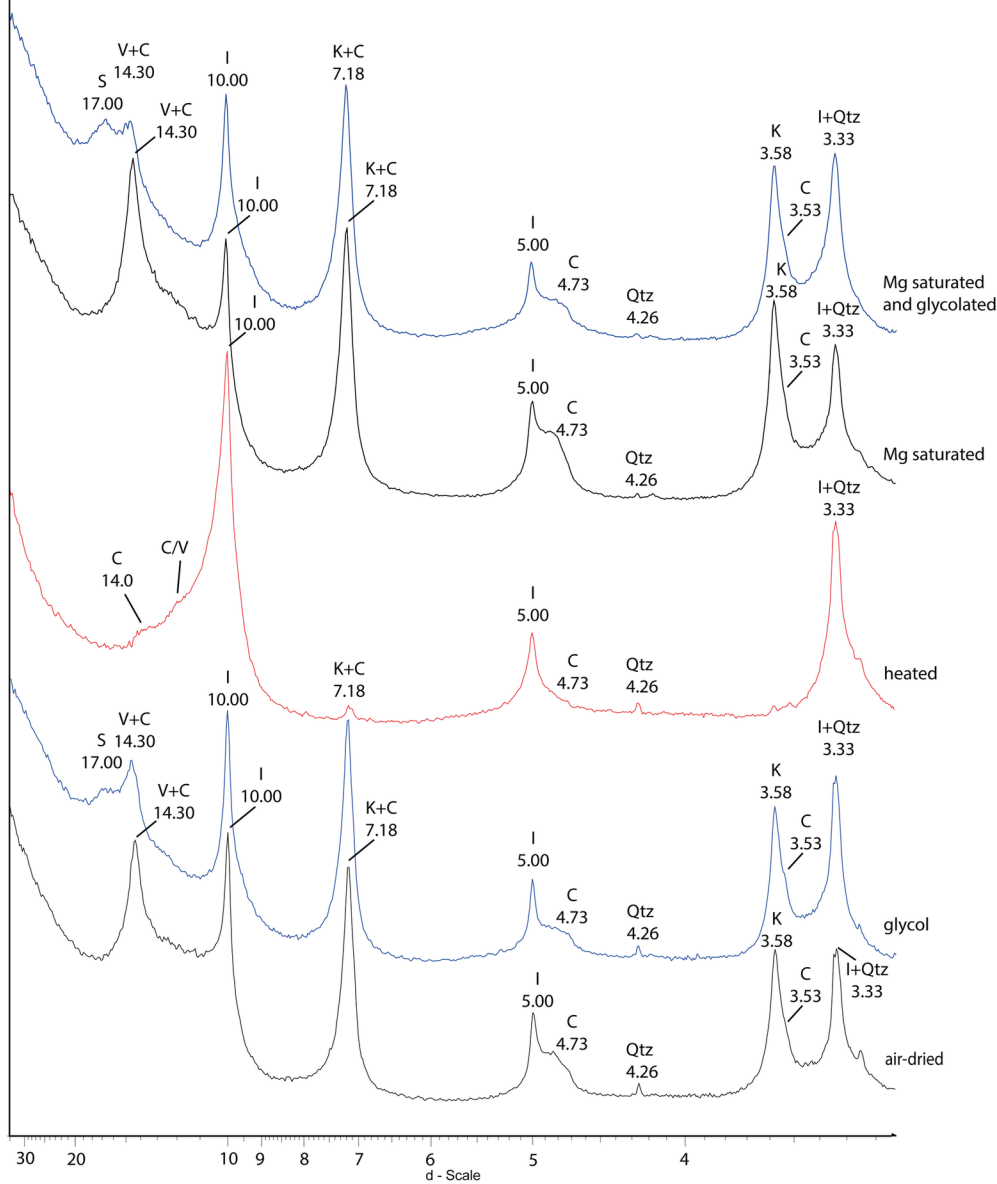


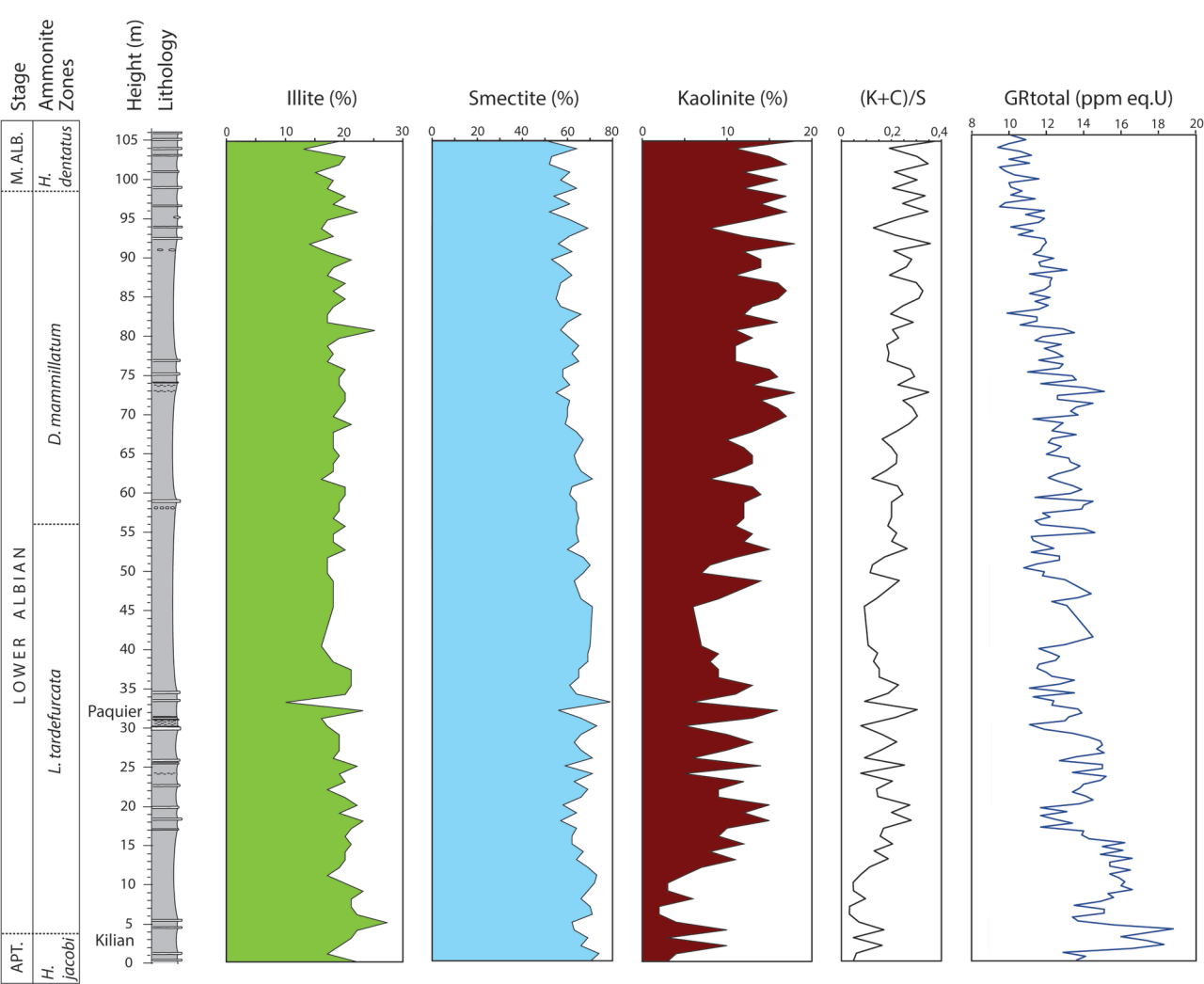
MIDDLE ALBIAN		UPPER ALBIAN	
<i>H. (Hopites) dentatus</i>	<i>Anahopites intermedius</i>	<i>Dim. riobe</i>	<i>Dimorphopites biplicatus</i>
Argiles tégluines de Courcelles			
Facies 2 - Silty clays		Facies 3 - Clays with limestones beds	
		<i>Mortoniceras (Mortoniceras) pricei</i>	<i>Mortoniceras (Mortoniceras) inflatum</i>
		Marmes de Brienne	
		Facies 4 - Marls	

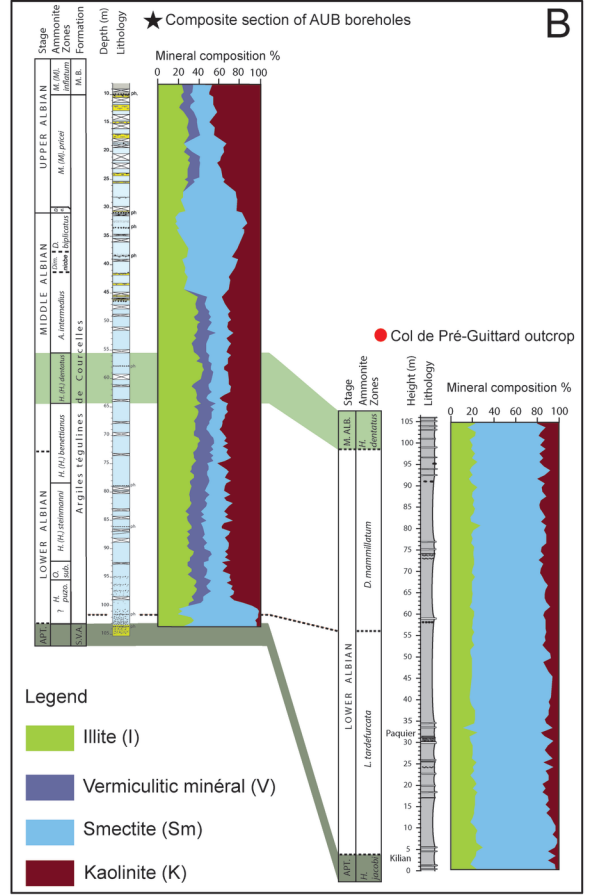
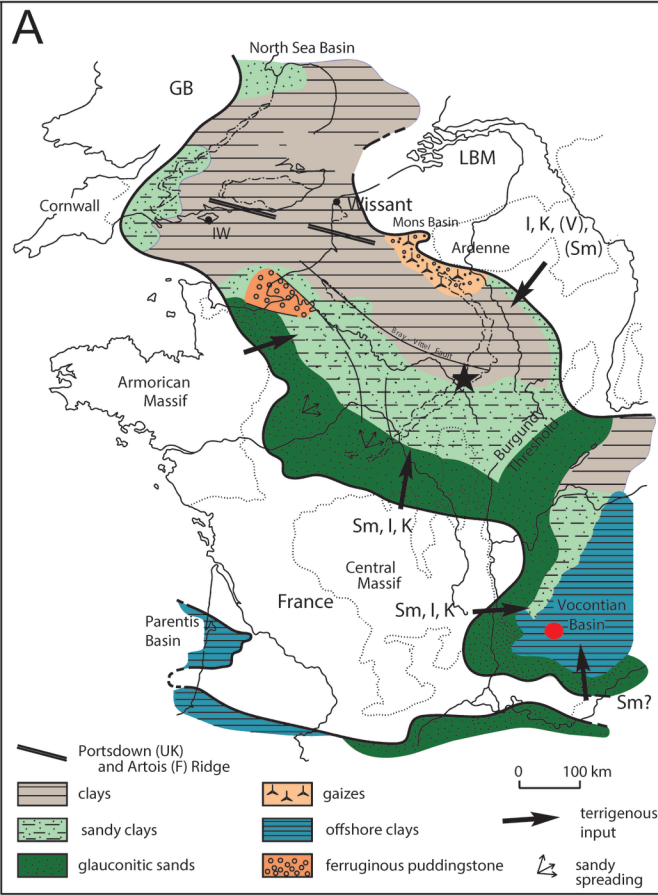
AUB 240











Stage	Boreal ammonite zonation (Amédro and Matrimon, 2014) (Paris Basin)	Tethyan ammonite zonation (Owen, 1999; Kennedy, 2000; Gale et al., 2011) (Vocontian Basin)
Upper Albian p.p.	<i>M. inflatum</i>	<i>M. inflatum</i>
	<i>M. pricei</i>	<i>M. pricei</i>
	<i>D. cristatum</i>	<i>D. cristatum</i>
Middle Albian	<i>D. biplicatus</i>	<i>O. roissyanum</i>
	<i>D. niobe</i>	
	<i>A. intermedius</i>	
	<i>H. dentatus</i>	
Lower Albian	<i>H. benettianus</i> $\frac{L.l.}{L.ps.}$	<i>L. lyelli</i>
	<i>H. steinmanni</i>	<i>D. mammillatum</i>
	<i>O. subhilli</i>	
	<i>H. puzosiana</i>	
	<i>C. floridum</i>	
	<i>S. kitchini</i>	<i>L. regularis</i>
	<i>L. regularis</i>	
	<i>L. tardefurcata</i>	
	<i>L. germanica</i>	
	U. Apt.	<i>L. schrammeni</i>
<i>H. jacobi</i>		